ASK1 contributes to fibrosis and dysfunction in models of kidney disease

John T. Liles,[1] Britton K. Corkey,[1] Gregory T. Notte,[1] Grant R. Budas,[1] Eric B. Lansdon,[1] Ford Hinojosa-Kirschenbaum,[1] Shawn S. Badal,[1] Michael Lee,[1] Brian E. Schultz,[1] Sarah Wise,[1] Swetha Pendem,[1] Michael Graupe,[1] Laurie Castonguay,[2] Keith A. Koch,[3] Melanie H. Wong,[1] Giuseppe A. Papalia,[1] Dorothy M. French,[1] Theodore Sullivan,[1] Erik G. Huntzicker,[1] Frank Y. Ma,[4] David J. Nikolic-Paterson,[4] Tareq Altuhaifi,[5] Haichun Yang,[6] Agnes B. Fogo,[6] and David G. Breckenridge[1]

[1]Gilead Sciences, Foster City, California, USA. [2]Ency2 Consulting, Denver, Colorado, USA. [3]Consortium for Fibrosis Research and Translation, University of Colorado Anschutz Medical Campus, Denver, Colorado, USA. [4]Department of Nephrology and Monash University Centres for Inflammatory Diseases, Monash Medical Centre, Clayton, Victoria, Australia. [5]College of Medicine, Alfaisal University, Riyadh, Saudi Arabia. [6]Department of Pathology, Microbiology and Immunology, Vanderbilt University Medical Center, Nashville, Tennessee, USA.

Oxidative stress is an underlying component of acute and chronic kidney disease. Apoptosis signal–regulating kinase 1 (ASK1) is a widely expressed redox-sensitive serine threonine kinase that activates p38 and c-Jun N-terminal kinase (JNK) mitogen-activated protein kinase kinases, and induces apoptotic, inflammatory, and fibrotic signaling in settings of oxidative stress. We describe the discovery and characterization of a potent and selective small-molecule inhibitor of ASK1, GS-444217, and demonstrate the therapeutic potential of ASK1 inhibition to reduce kidney injury and fibrosis. Activation of the ASK1 pathway in glomerular and tubular compartments was confirmed in renal biopsies from patients with diabetic kidney disease (DKD) and was decreased by GS-444217 in several rodent models of kidney injury and fibrosis that collectively represented the hallmarks of DKD pathology. Treatment with GS-444217 reduced progressive inflammation and fibrosis in the kidney and halted glomerular filtration rate decline. Combination of GS-444217 with enalapril, an angiotensin-converting enzyme inhibitor, led to a greater reduction in proteinuria and regression of glomerulosclerosis. These results identify ASK1 as an important target for renal disease and support the clinical development of an ASK1 inhibitor for the treatment of DKD.

Introduction

In developed countries, diabetic kidney disease (DKD) is the leading cause of end-stage renal disease, accounting for about 50% of incident cases (1, 2). The incidence and prevalence of DKD are on the rise as a result of the global diabetes epidemic (1, 2). Therapies for DKD target strict glycemic and blood pressure control and inhibition of the renin-angiotensin system (RAS). Despite these therapies, glomerular filtration rate (GFR) continues to decline in most patients (1–3). Progressive loss of GFR in DKD patients is the result of fibrosis in the glomerulus (glomerulosclerosis), which reduces the surface area available for filtration, and fibrosis in the tubulointerstitial compartment, which leads to atrophy, nephron dropout, and a reduction of total kidney mass (4, 5). A large unmet medical need remains for therapeutics that can halt progressive loss of kidney function by targeting pathological drivers of fibrosis and by providing benefit on top of current standard-of-care agents.

Oxidative stress (OS) promotes glomerulosclerosis and tubulointerstitial fibrosis in DKD (4, 6–11). OS is a pathological state caused by an imbalance in the production and clearance of reactive oxygen species (ROS). OS is elevated in the diabetic kidney because of mitochondrial dysfunction, hypoxia, increased inflammation, elevated activity of NADPH oxidases, and decreased expression of antioxidant proteins (11–13). OS causes sustained activation of redox-sensitive signal transduction pathways that promote loss of parenchymal cells through apoptosis and necrosis and that promote local production of inflammatory cytokines. Cell death and inflammation are signals for the recruitment and activation of myofibroblasts, the extracellular matrix–producing cells that cause progressive fibrosis in DKD (4, 10, 11, 14). Although numerous ROS scavengers have been proposed as therapeutics for DKD, they lacked specificity, potency, or adequate pharmaceutical properties to strongly inhibit ROS-mediated pathways implicated in DKD (12, 13). Additionally, the potential benefits of antioxidant therapies may have been masked by simultaneous interference with physiological ROS signaling (12, 13). Druggable targets are needed that will reduce the pathological consequences of OS while avoiding the nonspecificity of direct targeting of ROS.

Apoptosis signal–regulating kinase 1 (ASK1) is a ubiquitously expressed member of the mitogen-activated protein kinase kinase kinase (MAPKKK) family and a key regulator of OS-induced apoptosis, necrosis, inflammation, and fibrosis (15–17). ASK1 is normally bound and repressed by thiol-containing antioxidant proteins, including thioredoxin 1 (Trx1) in the cytosol and thioredoxin 2 (Trx2) in the mitochondria (18–20). In response to OS, thioredoxin undergoes oxidation and dissociation from ASK1, leading to trans-autophosphorylation of ASK1 homodimers at Thr845 within the activation loop (20, 21). Thr845-phosphorylated ASK1 has increased catalytic activity and phosphorylates MAPKKs 3, 4, 6,

Conflict of interest: JTL, BKC, GTN, EBL, GB, FHK, SSB, ML, SP, BS, SW, DF, TS, EH, MW, GAP, MG, and DGB are or were employees and/or shareholders of Gilead Sciences. LC, KAK, FYM, DJNP, TA, HY, and ABF received research reagents or financial support to conduct studies for Gilead Sciences.
Submitted: January 16, 2018; **Accepted:** July 13, 2018.
Reference information: *J Clin Invest*. 2018;128(10):4485–4500.
https://doi.org/10.1172/JCI99768.

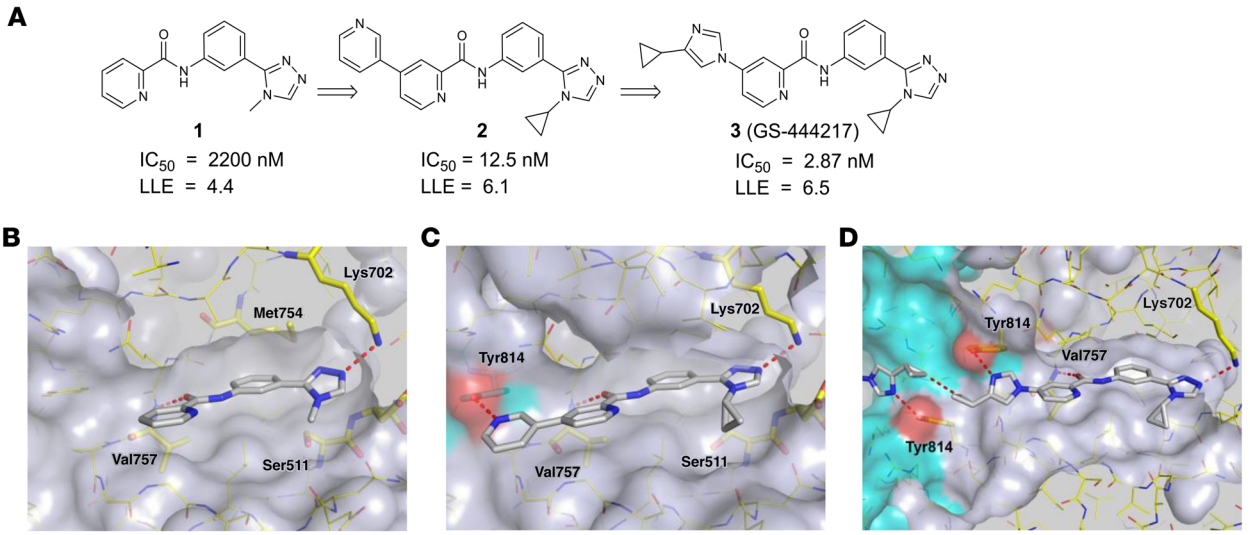

Figure 1. Structure-based drug design of compound 3, GS-444217. (**A**) Medicinal chemistry optimization of compound 1 showing improved biochemical potency (IC_{50}) and maintenance of low lipophilicity resulting in improved lipophilic ligand efficiency (LLE). (**B**) Structure of compound 1 occupying the ATP-binding pocket of ASK1. Interactions between hinge residue Val757 and the catalytic residue Lys709 are highlighted. (**C**) Structure of compound 2 bound to ASK1 with a cross-dimer interaction to the Tyr814 residue of the neighboring ASK1 monomer. (**D**) Structure of compound 3 (GS-444217) bound to ASK1.

and 7, which in turn phosphorylate and activate the MAPKs p38 and c-Jun N-terminal kinase (JNK) (17, 22). In response to pathological OS, ASK1 activation of p38 and JNK mediates diverse stress response pathways in cell type– and context-dependent manners. For example, in experimental models of acute and chronic renal disease, these downstream MAPKs drive inflammation, fibrosis, and apoptosis, and are implicated as contributors to kidney disease in humans (23–27). Indeed, p38 and JNK activity are increased in the renal vasculature, glomerulus, and tubulointerstitium of kidneys from diabetic and nondiabetic patients with chronic kidney disease (CKD) (28, 29). ASK1 is required for sustained activation of p38 and JNK; therefore, ASK1 serves as a mechanistic link between OS and the downstream pathological processes mediated by these 2 kinases (30).

Herein, we describe the discovery of a novel small-molecule inhibitor of ASK1 and demonstrate its therapeutic potential in rodent models of acute and chronic kidney injury. A medicinal chemistry hit-to-lead optimization effort resulted in GS-444217, a potent and selective ATP-competitive inhibitor of ASK1 in preclinical models. GS-444217 has low-nanomolar potency and is highly selective for ASK1 over other kinases. GS-444217 strongly suppressed the activation of ASK1, p38, and JNK in the kidney, resulting in decreased death of parenchymal cells, inflammation, and fibrosis. Importantly, combination of GS-444217 with a RAS inhibitor led to regression of fibrosis. These results confirm that ASK1 activation is a central mediator of kidney fibrosis and dysfunction and demonstrate that ASK1 inhibition represents a promising therapeutic approach for reducing the deleterious downstream consequences of OS in the kidney.

Results

Structure-based drug design of GS-444217. To identify inhibitors of ASK1, a library of approximately 100,000 compounds was screened against the ASK1 kinase domain using a competitive, time-resolved fluorescence resonance energy transfer immunoassay. A picolinamide derivative 1 (Figure 1, A and B) with moderate biochemical potency (IC_{50} = 2.2 μM) was selected for follow-up based on its low molecular weight and the chemical tractability of the aryl amide. To understand the binding mode of compound 1, the protein x-ray cocrystal structure was determined. By crystallography, the ASK1 kinase domain is a homodimer consisting of monomers arranged in a head-to-tail manner. The active sites of each monomer are on the same face of the protein and connected by a deep channel (Supplemental Figure 1; supplemental material available online with this article; https://doi.org/10.1172/JCI99768DS1). Compound 1 occupies the ATP-binding pocket of each ASK1 monomer and makes 2 hydrogen-bond interactions (Figure 1B). The triazole engages in a hydrogen bond to the catalytic residue Lys702 (2.8 Å), and an additional hydrogen bond (2.9 Å) occurs between the amide carbonyl of compound 1 and the backbone nitrogen of the hinge residue Val757. The nature of the hinge interaction was deemed a desirable feature of the inhibitor because amide carbonyls were, at the time, an underrepresented hinge-binding motif in kinase inhibitors, and a monodentate interaction with the highly conserved hinge region may avoid promiscuous interaction with other kinases.

Analysis of the binding mode of compound 1 revealed a hydrophobic pocket around the triazole *N*-methyl substituent that could be filled more effectively with larger groups. Replacing this substituent with cycloalkyl groups increased potency, with the *N*-cyclopropyl analog providing a 4-fold increase in potency (compound 9, see the Supplemental Note on Chemical Synthesis). Crystallography of compound 1 also revealed an open trajectory at the 4 position of the picolinamide ring. We found that most aromatic substituents were well tolerated, and introduction of a 3-pyridyl group provided a 52-fold potency improvement (compound 10, Supplementary Note on Chemical Synthesis). Compound 2 (Figure 1, A and C) arose through combination of

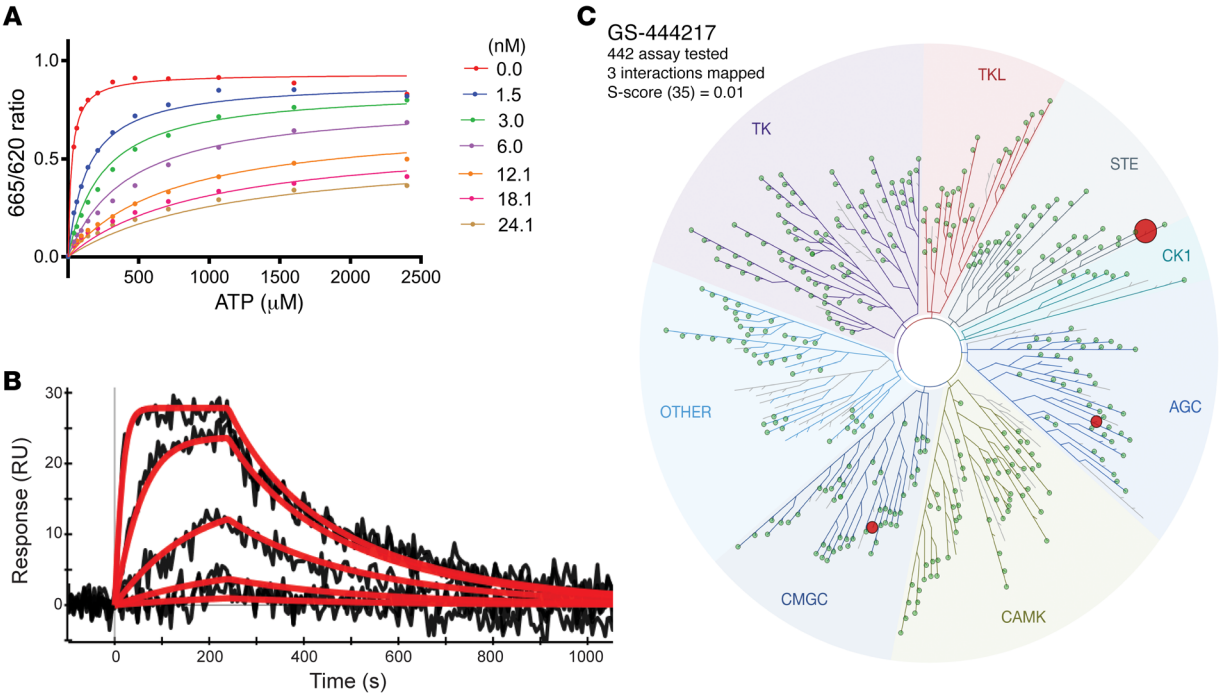

Figure 2. GS-444217, a selective ATP-competitive inhibitor of ASK1. (**A**) Enzymatic competition of GS-444217 with ATP was measured in the presence of increasing concentrations of GS-444217 (0–24 nM) and ATP (0–2,400 μM). (**B**) Kinetics and binding affinity of GS-444217 to ASK1 using surface plasmon resonance. Black traces represent the experimental data, and red traces represent the fit of a simple 1:1 interaction model to the data. (**C**) Selectivity of GS-444217 (1 μM) for ASK1 was determined using KINOME*scan* binding assay against 442 kinases. Map describes quantitatively the interaction patterns of GS-444217 with major kinase families: tyrosine kinases (TK), tyrosine kinase–like (TKL), serine/threonine kinases (STE), casein kinase 1 (CK1), protein kinases A, G, C (AGC), calmodulin/calcium-regulated kinases (CAMK), CDK/MAPK/GSK3/CLK (CMGC), and Other, consisting of many diverse families. The sphere radius corresponds to inhibitor affinity. Size of red dots shows relative affinity of GS-444217 for ASK1 (largest dot), ribosomal s6 kinase-4 (RSK4), and dual-specificity tyrosine phosphorylation–regulated kinase-1A (DYRK1A).

these preferred elements, and the resultant 176-fold potency improvement demonstrated the additive nature of the 2 modifications. The crystal structure of compound 2 (Figure 1C) revealed that the newly appended distal pyridine extends past the hinge motif and makes a hydrogen bond to Tyr814 in the opposing ASK1 monomer (2.4 Å). Because the cross-dimer interaction with Tyr814 was unique and substantially increased potency, we further optimized the nature of the H-bond acceptor. After extensive screening of aryl, heteroaryl, and heterocyclic substituents at this position, we found that *N*-aryl imidazoles maintained potency and improved solubility relative to the pyridine series. Incorporation of a 4-cyclopropyl substituent on the *N*-aryl imidazole led to the discovery of GS-444217 (compound 3; Figure 1, A and D), whose biochemical potency was improved more than 750-fold compared with compound 1.

GS-444217 maintains hydrogen bonds with Val757 and Lys709, and the *N*-cyclopropyl group of the triazole fills out the pocket made by residues Ser821, Asp822, Leu810, and Asn808 (Figure 1D). The imidazole ring, like the 3-pyridyl group of 2, extends past the hinge motif and picks up the cross-dimer hydrogen bond to Tyr814 (2.8 Å), while the distal cyclopropyl groups approach each other to within 3.3 Å (Figure 1D). GS-444217 displayed potent inhibition of ASK1 (IC_{50} = 2.87 ± 0.85 nM), good solubility at neutral pH, excellent permeability across Caco-2 monolayers, and good metabolic stability in hepatocytes (Supplemental Table 1). Based on these parameters, GS-444217 was selected for in vitro and in vivo characterization.

GS-444217 is a selective ATP-competitive inhibitor of ASK1 with favorable pharmacokinetic properties. The interaction of GS-444217 with the ATP-binding pocket of ASK1 suggests that this compound functions as an ATP-competitive inhibitor of the kinase domain. To confirm this mechanism of action, the enzymatic competition of GS-444217 with ATP was assessed in a kinase assay using a recombinant ASK1 catalytic domain. The enzyme reaction rate was measured in the presence of increasing concentrations of GS-444217 and ATP (Figure 2A). The data fit yielded the following values for the key kinetic parameters: K_m (ATP) = 25 ± 2.5 μM, K_i = 0.32 ± 0.03 nM, and α = 111 ± 24. Based on the high α value, GS-444217 was deemed an ATP-competitive inhibitor (31). Next, a surface plasmon resonance–based ProteOn biosensor platform was used to characterize the kinetics and binding affinity of GS-444217 to ASK1. The sensorgrams show a profile of GS-444217 binding to ASK1 that is saturable, dose-responsive, and reversible (Figure 2B). Fitting yielded a relatively fast k_{on} of $1.9 \times 10^6 \pm 5.0 \times 10^5$ $M^{-1}s^{-1}$ and a moderately slow k_{off} of $5.2 \times 10^{-3} \pm 7.5 \times 10^{-4}$ s^{-1} resulting in a K_D of 2.9 ± 0.8 nM.

To evaluate the selectivity of binding to other kinases, GS-444217 (1 μM) was screened against a panel of 442 unique human kinases (KINOME*scan* platform), and K_D values were generated. GS-444217 demonstrated high selectivity for binding to

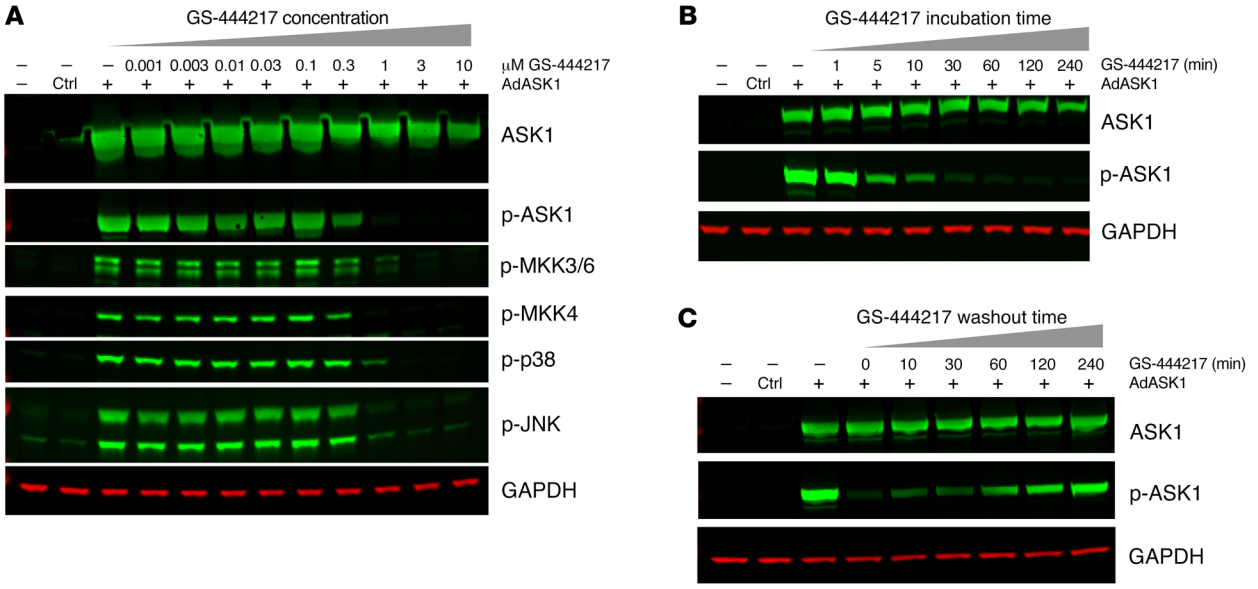

Figure 3. GS-444217 dose-dependently inhibits ASK1 activity. ASK1 inhibition assays using HEK293T cells with adenoviral overexpression of human ASK1 (AdASK1). (**A**) Cells were treated for 2 hours with 1:3 dilutions of GS-444217 (0.001–10 μM). Phosphorylation of ASK1 and ASK1 substrates (MKK3/6, MKK4, and their respective downstream substrates p38 and JNK kinases) was measured by Western blot. GAPDH was used as a protein-loading control. (**B**) Time course of ASK1 inhibition following treatment of cells with 1 μM GS-444217 (treatment duration of 1 minute to 4 hours). (**C**) Reversibility of ASK1 inhibition following washout of GS-444217 and replacement with serum-free media (washout time of 0–240 minutes).

ASK1 versus the other kinases in the panel (Figure 2C). The affinity of GS-444217 for ASK1 (K_D = 4.1 nM) was 53-fold greater than the affinity for dual-specificity tyrosine phosphorylation–regulated kinase-1A (DYRK1A, K_D = 220 nM) and 104-fold greater than the affinity for ribosomal s6 kinase-4 (RSK4, K_D = 430 nM), the 2 off-target kinases identified (Figure 2C).

To evaluate pharmacokinetic (PK) properties and tolerability, GS-444217 was administered to rats orally at 10 or 30 mg/kg. GS-444217 demonstrated excellent oral bioavailability and dose linearity; however, the plasma half-life was not sufficient to support once-daily dosing (Supplemental Figure 2A and Supplemental Table 2). Sustained plasma levels could be achieved with GS-444217 mixed into rodent chow (Supplemental Figure 2, B, C, and D), and GS-444217 was well tolerated in this formula by rats and mice. Collectively, GS-444217 is a potent, selective, and reversible ATP-competitive inhibitor of ASK1 with favorable PK properties upon oral administration.

GS-444217 inhibits ASK1 autophosphorylation and phosphorylation of p38 and JNK MAP kinases. The effect of GS-444217 to inhibit ASK1 autophosphorylation and ASK1-mediated signaling was evaluated in cell-based assays. First, adenoviral overexpression of human ASK1 in HEK293T cells induced ASK1 autophosphorylation at Thr838 (a marker of ASK1 activity; refs. 15, 16) and induced phosphorylation of the ASK1 substrates MKK3/6 and MKK4 and their downstream substrates p38 and JNK (Figure 3A). Treatment with GS-444217 reduced ASK1 phosphorylation and prevented the phosphorylation of MKK3/6, MKK4, p38, and JNK at concentrations of 0.3 μM and above with full suppression of ASK1 activity at 1 μM. GS-444217 reduced ASK1 activity within 5 minutes of addition to the cultures, reaching a maximum level of inhibition by 30 minutes (Figure 3B). Removal of GS-444217 from the cultures resulted in reactivation of ASK1 autophosphorylation within 10 minutes and near-complete recovery 2 hours after drug washout (Figure 3C). Next, the inhibitory activity of GS-444217 was evaluated in rat neonatal ventricular cardiomyocytes and in human renal proximal tubular epithelial cells (HK-2) undergoing OS. GS-444217 inhibited the activation of endogenous ASK1 and p38 in cardiomyocytes treated with auranofin (thioredoxin reductase inhibitor), 2-acetylamino-3-[4-(2-acetylamino-2-carboxyethylsulfanylthiocarbonylamino) phenylthiocarbamoylsulfanyl] propionic acid (2-AAPA, glutathione reductase inhibitor), or diethyldithiocarbamate (DDC, superoxide dismutase inhibitor) and in HK-2 cells treated with H_2O_2 (Supplemental Figure 3, A–D). In summary, GS-444217 causes rapid, reversible, and dose-dependent inhibition of ASK1 activity and ASK1-dependent signaling of downstream MAP kinases.

The BioMAP Diversity PLUS panel (Supplemental Figure 4A) was used to determine the specificity of GS-444217 for ASK1 signaling compared with a selective p38 inhibitor (BIRB-796) in primary human cells. At a concentration of 1 μM, a dose that suppresses ASK1 and p38 activation in HEK293T cells, the only pharmacological effect of GS-444217 was mild suppression of TNF-α production in B cells, an expected pharmacology for an ASK1 inhibitor (32). The high degree of specificity of GS-444217 contrasted with the effects of BIRB-796 (Supplemental Figure 4B). Further, GS-444217 was not cytotoxic at any concentration tested (0.1 to 10 μM). These results are consistent with a role for ASK1 in mediating activation of p38 and JNK by pathological stress signals, but not physiological signals mediated by receptor kinases.

GS-444217 reduces OS-induced ASK1 signaling in kidney and inhibits acute renal tubular injury in rats. To assess the ability of GS-444217 to block ASK1 activation and signaling in kidney and

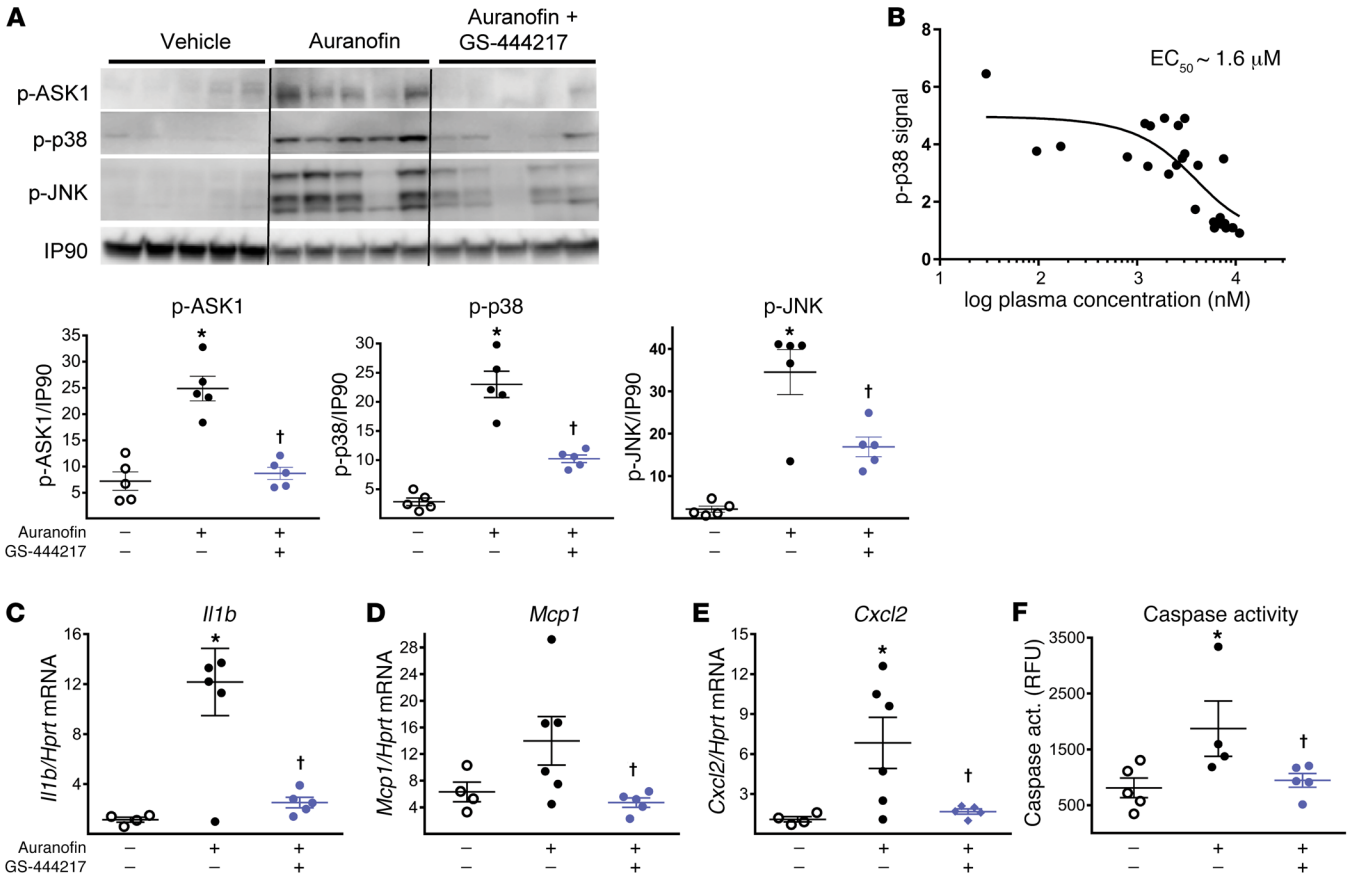

Figure 4. GS-444217 inhibits activation of ASK1, p38, and JNK in rat kidney. (**A** and **C**–**F**) A single oral dose of GS-444217 (30 mg/kg, $n = 8$) or vehicle (equal volume, $n = 5$) was administered to Sprague-Dawley rats, which were challenged 30 minutes later with auranofin (30 mg/kg, i.p.) to cause OS-induced activation of the ASK1 pathway. Kidney cortex samples were collected 30 minutes after auranofin administration. (**A**) Western blot analysis of renal cortex lysates showing p-ASK1, p-p38, and p-JNK levels after in vivo administration of vehicle, auranofin, or auranofin and 30 mg/kg GS-444217. Dot plots show p-ASK1, p-p38, and p-JNK levels normalized to IP90 loading control. (**B**) GS-444217 (10 mg/kg, $n = 14$, or 30 mg/kg, $n = 12$, p.o.) was administered to Sprague-Dawley rats. Plasma was collected from individual rats over the course of the dosing interval, and kidneys were collected at the end of the time course. Based on plasma concentrations of GS-444217 and the corresponding p-p38 signal in each kidney (measured by ELISA in renal cortex lysates), the in vivo EC_{50} of GS-444217 for inhibition of the renal ASK1 pathway was estimated to be 1.6 μM. (**C**–**F**) Relative mRNA expression of inflammatory cytokines (*Il1b*, *Ccl2*, and *Cxcl2*) and caspase activity were measured in kidneys of rats treated with vehicle, auranofin, or auranofin and 30 mg/kg GS-444217. RFU, relative fluorescence units. For **A** and **C**–**F**, data are mean ± SEM; $^{*}P < 0.01$ vs. control, $^{\dagger}P < 0.01$ vs. auranofin (ANOVA with Bonferroni's multiple-comparisons test).

to characterize the resultant biological effects, we established an acute pharmacodynamic model of OS by administrating auranofin to rats (Supplemental Figure 5A). Auranofin inhibits thioredoxin reductase, leading to immediate oxidation of thioredoxin and activation of ASK1 (20, 21, 33). Auranofin dose-dependently increased activation of ASK1, p38, and JNK in the kidney within 30 minutes of injection and induced *Il1b* mRNA expression and caspase-3 activity (Supplemental Figure 6, A–E). One dose of GS-444217 (30 mg/kg) given 30 minutes before administration of auranofin (30 mg/kg) suppressed the activation of ASK1, p38, and JNK in renal cortex (Figure 4A). Auranofin administration induced mRNA expression of inflammatory cytokines (*Il1b*, *Ccl2*, and *Cxcl2*) and increased caspase activity in kidney, and these downstream effects of ASK1 activation were inhibited by GS-444217 (Figure 4, C–F). Comparing plasma concentrations of GS-444217 with the corresponding phosphorylated p38 (p-p38) signal in kidney, GS-444217 had an in vivo EC_{50} of approximately 1.6 μM for inhibiting the ASK1 pathway in rodent kidney (Figure 4B). These data were used to select doses for animal-efficacy studies so that the EC_{50} of GS-444217 would be covered at trough plasma levels.

OS in the kidney is known to cause tubular necrosis, tubulointerstitial apoptosis, inflammation, and fibrosis (4, 6–11). $ASK1^{-/-}$ mice are protected against tubular injury caused by renal ischemia/reperfusion (I/R) and from tubulointerstitial inflammation and fibrosis caused by unilateral ureteral obstruction (UUO) (23, 34), suggesting that ASK1 is important for mediating tubular injury and fibrosis. Protection against tubular injury by GS-444217 was tested in an acute kidney injury model of renal I/R in rats. GS-444217 (30 mg/kg) was orally administered immediately before a 30-minute period of bilateral renal ischemia, and renal dysfunction was evaluated in serum and kidneys following a 24-hour reperfusion period (Supplemental Figure 5B). In comparison with vehicle-treated rats, 1 dose of GS-444217 reduced creatinine and blood urea nitrogen in serum (Figure 5, A and B), decreased tubular necrosis measured by

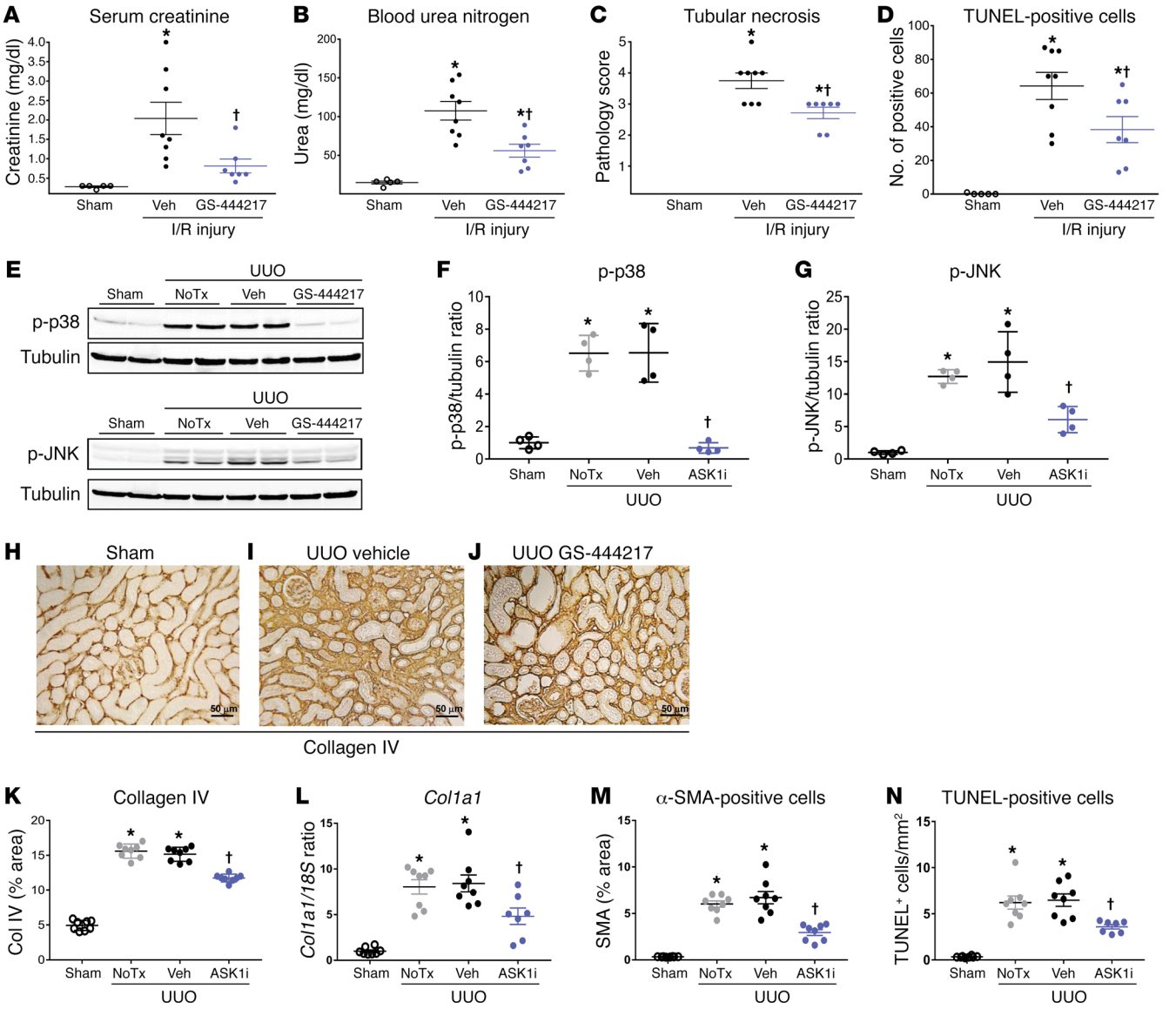

Figure 5. GS-444217 inhibits acute renal tubular injury in rat kidney. (**A**–**D**) Renal ischemia/reperfusion (I/R) injury. GS-444217 (30 mg/kg) or vehicle (Veh; equal volume) was orally administered to Sprague-Dawley rats just before 30 minutes of bilateral renal ischemia. Parameters of renal function were assessed in serum and kidney following a 24-hour reperfusion period. (**A** and **B**) Serum creatinine and blood urea nitrogen concentrations. (**C** and **D**) Renal pathology scores for tubular necrosis (H&E-stained sections) and apoptosis/necrosis (TUNEL stain). Data in **A**–**D** are mean ± SEM, n = 5–8; *P < 0.05 vs. control, †P < 0.05 vs. I/R treated with vehicle (ANOVA with Bonferroni's multiple-comparisons test). (**E**–**N**) Unilateral ureteral obstruction (UUO). Sprague-Dawley rats had sham or UUO surgery. GS-444217 (30 mg/kg) or vehicle (equal volume) was orally administered 1 hour before surgery and continued twice per day for 7 days. (**E**–**G**) Western blot analysis of kidney lysates for p-p38 and p-JNK. Dot plots show p-p38 and p-JNK levels normalized to tubulin loading control (NoTx, no treatment). (**H**–**K**, **M**, and **N**) Image analysis and graphed pathology scores of renal sections stained for collagen deposition (collagen IV) (scale bars: 50 μm) (**H**–**K**), cortical interstitial α-smooth muscle actin–positive (α-SMA–positive) myofibroblasts (**M**), and apoptosis/necrosis of kidney epithelial cells (TUNEL) (**N**). (**L**) Collagen I (*Col1a1*) mRNA was measured in whole kidney by reverse transcriptase PCR. Data in **F**, **G**, and **K**–**N** are mean ± SEM, n = 4 (sham), n = 8 (UUO); *P < 0.01 vs. sham surgery, †P < 0.01 vs. UUO treated with vehicle (ANOVA with Bonferroni's multiple-comparisons test).

pathology (Figure 5C and Supplemental Figure 7), and decreased tubular cell apoptosis measured by TUNEL staining (Figure 5D and Supplemental Figure 7). GS-444217 administration also decreased mRNA expression of several proinflammatory and profibrotic mediators in the kidney, including *Ccl2*, *Cxcl2*, *Il1b*, *Il6*, *Tnfa*, and *Tgfb1* (Supplemental Figure 8).

The efficacy of GS-444217 to reduce ASK1-mediated kinase activation, tubular epithelial cell death, interstitial inflammation, and fibrosis in kidney was tested in a 7-day UUO model in rats (Supplemental Figure 5C). In comparison with sham rats without UUO, p-p38 and p-JNK levels were elevated in obstructed kidneys and were reduced by GS-444217 orally administered at 30 mg/kg twice per day (Figure 5, E–G). Activation of ASK1 during UUO was reduced by oral administration of GS-444217 (Supplemental Figure 9A). As expected, GS-444217 did not affect the activation of the related MAP kinase ERK (data not shown). UUO caused increases in markers of fibrosis such as collagen IV deposition (Figure 5, H–K), collagen I (*Col1a1*) mRNA expression (Figure

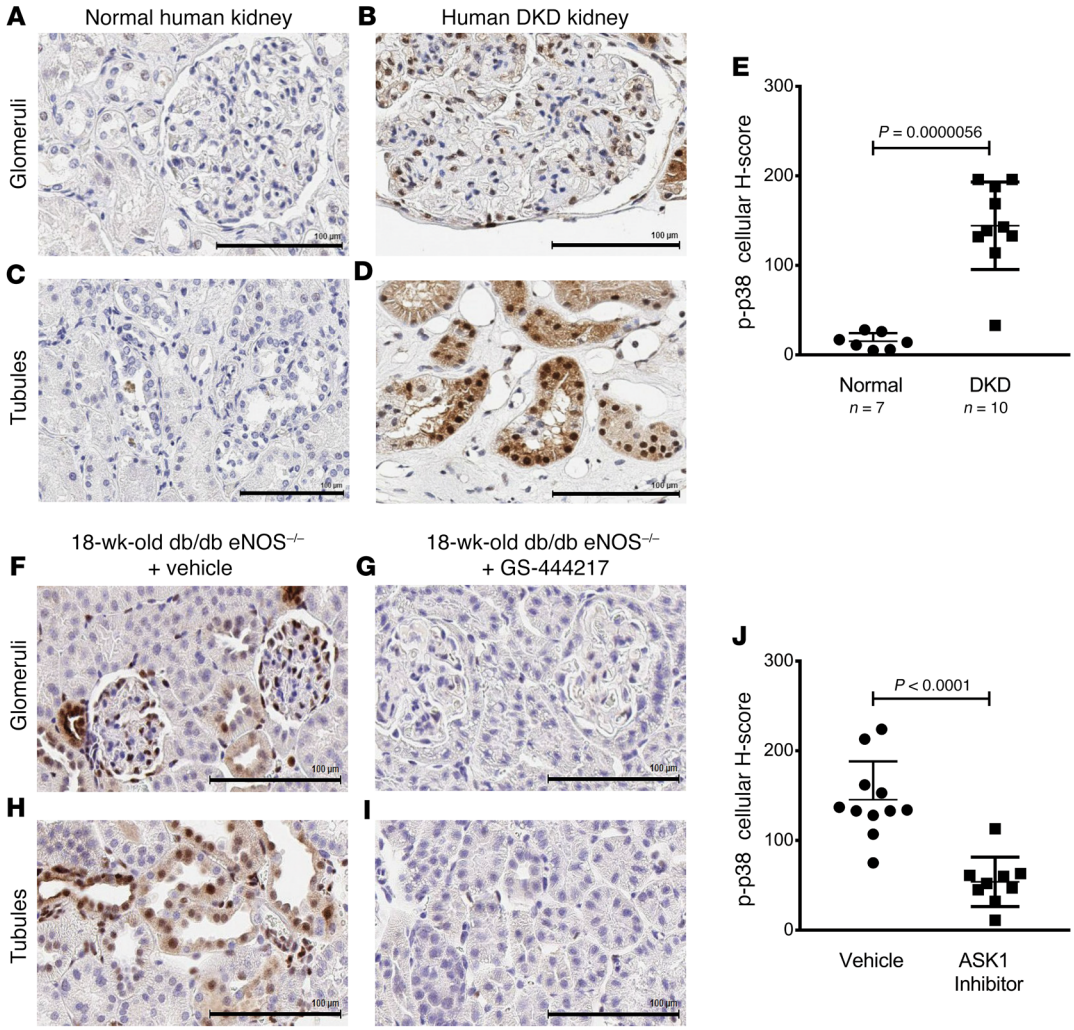

Figure 6. The ASK1 pathway is activated similarly in DKD patients and db/db eNOS$^{-/-}$ mice. (**A**–**J**) Immunostaining for p-p38 was used as a measure of ASK1 pathway activation in kidney biopsies from donors without kidney disease ("normal," n = 7) (**A** and **C**) and patients with DKD (n = 10) (**B** and **D**), and kidneys from 18-week-old db/db eNOS$^{-/-}$ mice treated with vehicle (standard rodent chow) (**F** and **H**) or with GS-444217 (0.3% in rodent chow) (**G** and **I**) for 8 weeks (n = 8–10). Representative images of glomerular (top panels) and tubulointerstitial compartments (bottom panels) are shown for human and mouse (scale bars: 100 μm). (**E** and **J**) Whole-slide images were analyzed with Definiens Developer XD and expressed as an H-Score that quantifies p-p38 staining intensity and distribution in kidney biopsies from DKD patients and controls (**E**) and in kidneys from 18-week-old db/db eNOS$^{-/-}$ mice treated with vehicle or with GS-444217 for 8 weeks (**J**) (mean ± SD; P value is shown on graph; unpaired t test).

5L), total collagen (Supplemental Figure 9C), cortical interstitial α-smooth muscle actin–positive (α-SMA–positive) myofibroblasts (Figure 5M), tubular epithelial cell death (TUNEL-positive cells) (Figure 5N and Supplemental Figure 9B), and positive staining with Masson's trichrome (Supplemental Figure 9D). Treatment of UUO rats with GS-444217 reduced these measures of tubular injury and fibrosis and associated expression of profibrotic genes (e.g., connective tissue growth factor [*Ctgf*], plasminogen activator inhibitor [*Serpine1*], and *Tgfb1*) (Supplemental Figure 10, C–E).

Based on results in models of acute kidney injury in rats, pharmacological inhibition of ASK1 with GS-444217 reduces OS-induced ASK1 signaling, which in turn preserves renal function by decreasing tubulointerstitial cell death, inflammation, and fibrosis.

ASK1 pathway is elevated in human DKD, and GS-444217 halts progressive loss of renal function in a mouse model of DKD. DKD is associated with OS, inflammation, and glomerular and interstitial fibrosis, ultimately leading to progressive loss of kidney function. We evaluated the level of ASK1 pathway activation by measuring p-p38 by immunohistochemistry on renal biopsies from patients with DKD (glomerular injury score of 2.11 ± 1.14 and interstitial fibrosis score of 2.38 ± 1.06) and from tissue donors without DKD (Supplemental Figure 11, A–C). Immunoreactivity of p-p38 was increased in the glomerulus and tubulointerstitium of patients with DKD compared with non-DKD kidneys (cellular H-score of 144.3 ± 48.85 vs. 15.29 ± 9) (Figure 6, A–E). Immunoreactivity of p-p38 was identified in mesangial areas, podocytes, parietal epithelial cells, and tubule epithelial cells (Supplemental Figure 12A) and was prominent in regions of tubulointerstitial fibrosis (Supplemental Figure 12B), a histological feature that is associated with GFR decline and progression to end-stage renal disease in patients with established DKD (5, 35–37). A newly developed p-ASK1 antibody was used to con-

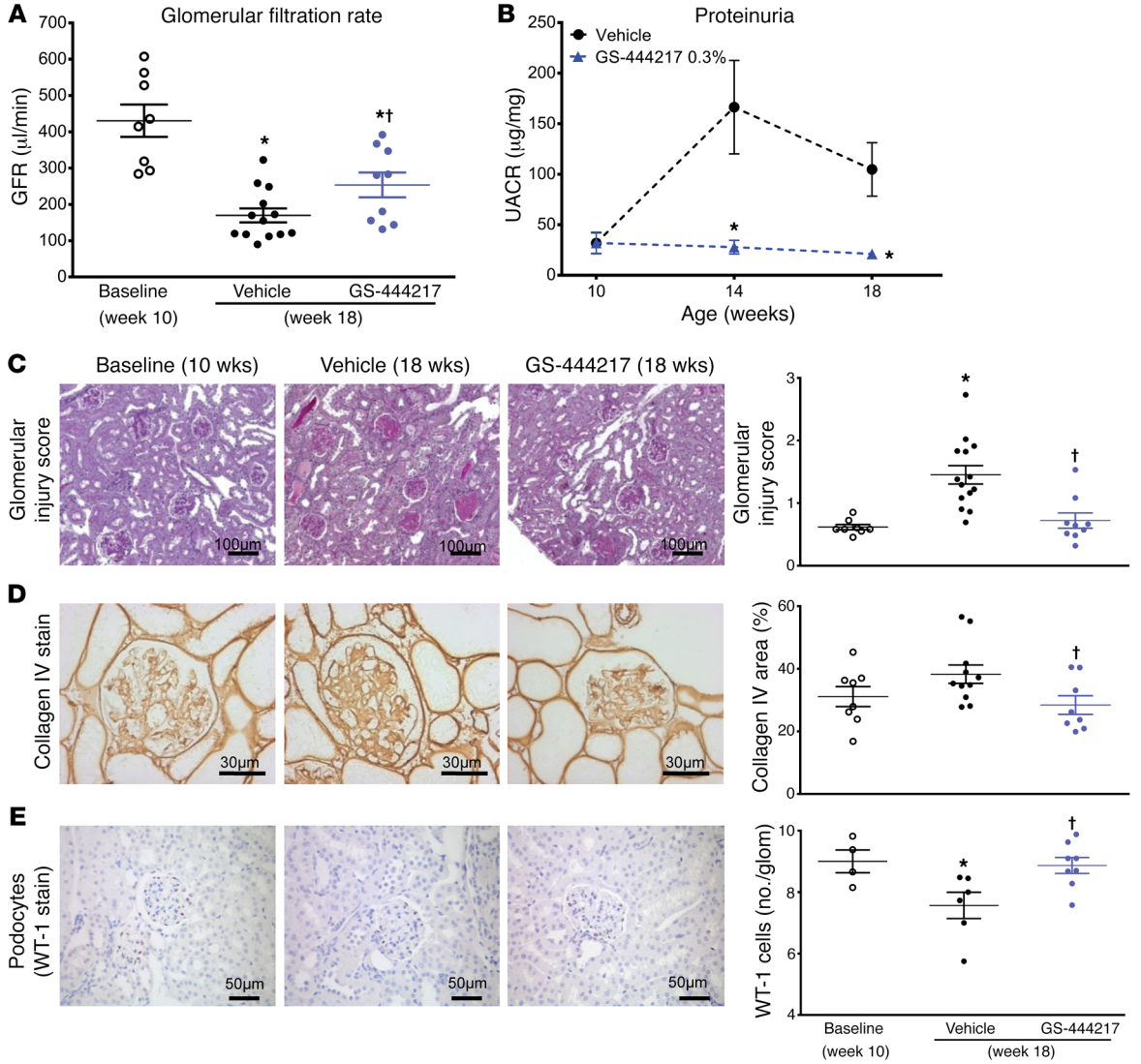

Figure 7. GS-444217 halts the progressive decline of renal function in a mouse model of DKD. (**A**–**E**) Ten-week-old db/db eNOS$^{-/-}$ mice were fed standard rodent chow (vehicle) or chow containing GS-444217 (0.3% by weight) for 8 weeks. A separate group of untreated db/db eNOS$^{-/-}$ mice were euthanized at 10 weeks of age to establish baseline-disease parameters. (**A**) GFR was measured using inulin-FITC clearance in baseline mice (week 10) and in treated mice (week 18). (**B**) Proteinuria (urinary albumin to creatinine ratio [UACR]) was measured at weeks 10, 14, and 18. (**C**) A sclerosis injury score was calculated at 18 weeks on periodic acid–Schiff–stained kidneys averaging the lesion scores of 80–100 glomeruli per mouse using the following scoring system: 0, no lesion; 1, sclerosis of up to 25% of the glomerulus; 2, sclerosis of 25%–50%; 3, sclerosis of 50%–75%; and 4, sclerosis of >75% of the glomerulus. (**D** and **E**) Image analysis and graphed pathology scores of renal sections stained for collagen deposition (collagen IV) (**D**) or podocyte loss (Wilms tumor antigen [WT-1]) (**E**). Scale bars: 100 μm (**C**), 50 μm (**E**), or 30 μm (**D**). Data in **A**–**E** are mean ± SEM, n = 9–12; *P < 0.05 vs. 10-week baseline by unpaired t test, †P < 0.05 vs. vehicle (ANOVA with Bonferroni's multiple-comparisons test).

firm ASK1 activation in the same cell types of DKD kidneys (Supplemental Figure 13).

To determine the utility of an ASK1 inhibitor as a therapy for DKD, we evaluated the efficacy of GS-444217 in a progressive model of DKD using db/db eNOS$^{-/-}$ mice, which have pathological features similar to human DKD such as functional, structural, and transcriptomic changes within the kidney, and ASK1 pathway activation (38–41). db/db eNOS$^{-/-}$ mice develop an initial phase of hyperfiltration, mesangial expansion, and modest glomerulosclerosis at 6–10 weeks of age, followed by a period of progressive decline in renal function (38, 41). The intensity and cellular distribution of p-p38 immunoreactivity in 18-week-old db/db eNOS$^{-/-}$ mice were similar to the levels seen in the human DKD kidneys (H-score = 145.36 ± 42.8 db/db eNOS$^{-/-}$ mice vs. 144.3 ± 48.85 human DKD) (Figure 6, E and J), demonstrating that this is a clinically relevant model to evaluate the efficacy of an ASK1 inhibitor. Ten-week-old db/db eNOS$^{-/-}$ mice were fed rodent chow without or with GS-444217 (0.3% by weight) for 8 weeks (Supplemental Figure 5D). GFR, as assessed by inulin-FITC clearance, decreased by 60% between weeks 10 and 18 in vehicle-treated db/db eNOS$^{-/-}$ mice. The decline in GFR was attenuated by treatment of mice with GS-444217 (Figure 7A). GS-444217 treatment blocked the increase in albuminuria that occurred between weeks 10 and 18 (Figure 7B) and reduced other pathological features of DKD in

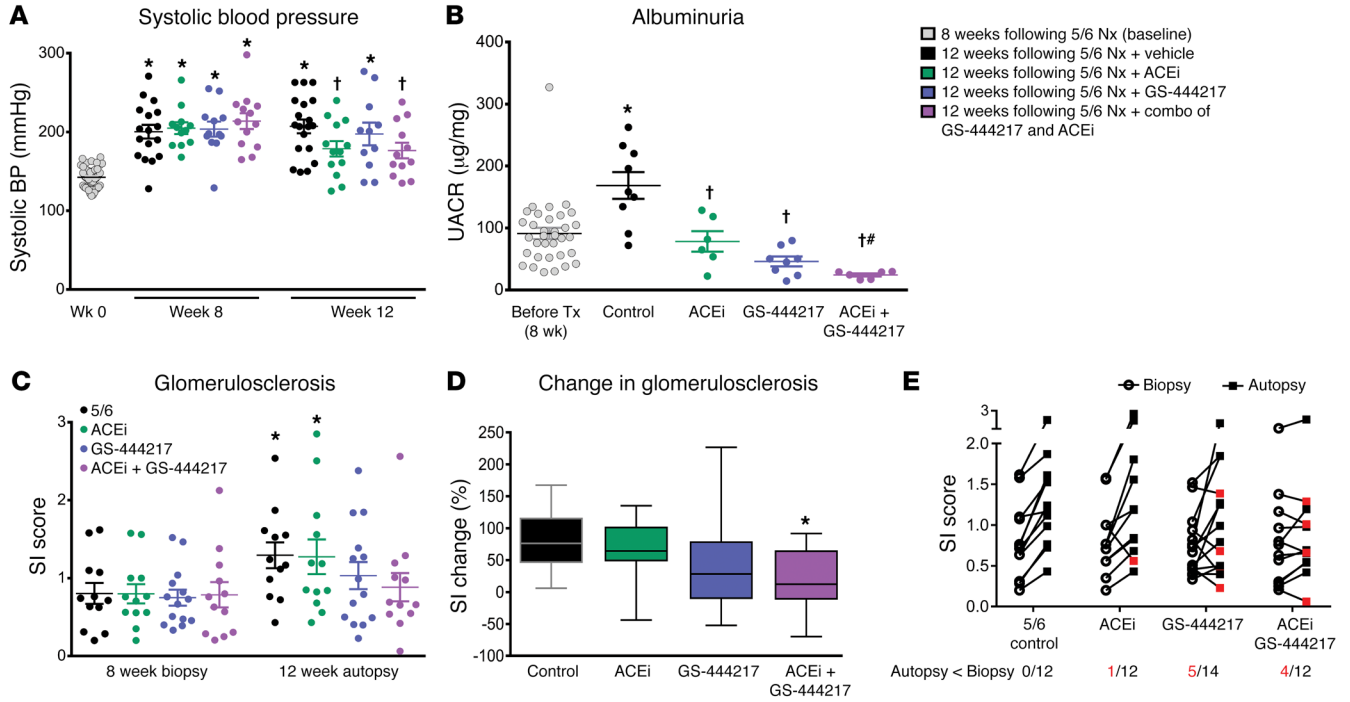

Figure 8. GS-444217 increases the efficacy of enalapril in a chronic glomerular injury model. (**A**–**E**) Eight weeks after 5/6 nephrectomy (5/6 Nx), Sprague-Dawley rats were randomized into groups based on sclerosis index (SI) scores determined from kidney biopsies and fed standard rodent chow (control), chow containing GS-444217 (0.3% by weight plus 30 mg/kg, once per day, p.o.), the angiotensin-converting enzyme inhibitor (ACEi) enalapril (50 mg/l in drinking water), or enalapril with GS-444217 for 4 weeks. (**A**) Systolic blood pressure (BP) was measured at week 0 (gray dots) and 8 and 12 weeks after Nx (black dots, control; green dots, ACEi; blue dots, GS-444217; purple dots, ACEi plus GS-444217). (**B**) Urinary albumin to creatinine ratio (UACR) before treatment (gray dots, averaged for all groups 8 weeks after Nx) or 4 weeks after Nx and treatment. (**C**–**E**) Glomerulosclerosis severity was measured by biopsy (8 weeks after Nx) or on whole kidney sections (12 weeks after Nx). (**C**) SI score was calculated on periodic acid–Schiff–stained kidney sections averaging the lesion scores of 80–100 glomeruli per rat (scoring system: 0, no lesion; 1, sclerosis of up to 25% of the glomerulus; 2, sclerosis of 25%–50%; 3, sclerosis of 50%–75%; 4, sclerosis of >75%). (**D**) Progression of glomerulosclerosis from week 8 to week 12 (box and whisker plot, minimum to maximum). (**E**) Before-and-after plots of SI scores at 8 weeks after Nx (biopsy; circles) and 12 weeks after Nx (autopsy; squares). Red squares indicate which rats showed regression of glomerulosclerosis from biopsy to autopsy. Numbers of rats (red font) per group in which glomerulosclerosis regressed are shown below the *x* axis. Data in **A**–**E** are mean ± SEM, $n = 12$–14; $^{*}P < 0.05$ vs. 8-week baseline by unpaired *t* test, $^{\dagger}P < 0.05$ vs. vehicle (ANOVA with Bonferroni's multiple-comparisons test); $^{\#}P < 0.01$ vs. GS-444217 or ACEi monotherapy (unpaired *t* test).

18-week-old db/db eNOS$^{-/-}$ mice such as glomerulosclerosis (Figure 7, C and D), loss of podocytes (Figure 7E), and tubulointerstitial fibrosis and apoptosis (Supplemental Figure 14, A and B). Urinary concentrations of the OS marker 8-isoprostane were reduced in 18-week-old db/db eNOS$^{-/-}$ mice treated with GS-444217 (Supplemental Figure 14C), indicating that GS-444217 reduces feed-forward ROS amplification pathways. We also characterized urinary biomarkers associated with human DKD progression in 18-week-old db/db eNOS$^{-/-}$ mice. ASK1 inhibition increased concentrations of urinary epidermal growth factor (EGF), a marker shown to strongly correlate with GFR decline in humans (Supplemental Figure 14D) (42). ASK1 inhibition also decreased markers related to inflammation and fibrosis (urinary tissue inhibitor of metalloproteinases 1 [TIMP-1]) and tubule injury (kidney injury molecule 1 [KIM-1]) (Supplemental Figure 14, E and F) (43, 44).

Immunohistochemistry analysis of kidneys from 10-week-old db/db eNOS$^{-/-}$ mice showed that p-p38 was present in podocytes and mesangial, endothelial, and tubulointerstitial cells and was further increased by 18 weeks as disease progressed (Figure 6, F and H). GS-444217 treatment strongly reduced p-p38 staining in all kidney-cell types (Figure 6, G and I) and reduced p-ASK1, p-p38, and p-JNK in kidney lysates (Supplemental Figure 15, A–C) from 18-week-old db/db eNOS$^{-/-}$ mice. In addition to inhibiting progression of renal disease, treatment of db/db eNOS$^{-/-}$ mice with GS-444217 was well tolerated as indicated by unaltered body weight and blood pressure (Supplemental Figure 16, A and B). A statistically significant decrease in hemoglobin A1C was detected in db/db eNOS$^{-/-}$ mice treated with GS-444217; however, this decrease was not accompanied by an alteration in fasting blood glucose (Supplemental Figure 16, C and D).

In summary, ASK1 inhibition by GS-444217 can halt the progressive decline in GFR and decrease proteinuria in a preclinical setting of established DKD by reducing apoptosis and fibrosis within the glomerular and tubulointerstitial compartments and by preserving podocyte density.

Combination of GS-444217 with angiotensin-converting enzyme inhibition has greater benefit than monotherapy in a chronic glomerular injury model. Inhibitors of RAS are the mainstay of CKD treatment and have been shown to reduce disease progression and improve survival of patients with CKD and DKD (3). Experiments in the rat 5/6 nephrectomy model (5/6 Nx) initially established that chronic RAS inhibition lowers systemic and intraglo-

merular pressures, leading to a reduction in glomerulosclerosis and albuminuria and to the preservation of renal function (45). We hypothesized that ASK1 inhibition represents an orthogonal therapeutic approach that could increase the efficacy of RAS inhibition in the 5/6 Nx model. Rats were randomized into treatment groups based on sclerosis index scores determined from kidney biopsies from rats at 8 weeks after Nx: (a) vehicle control, (b) the angiotensin-converting enzyme inhibitor enalapril (antihypertensive dose of 50 mg/l in drinking water), (c) GS-444217 (0.3% in chow and 30 mg/kg once per day orally to cover the in vivo EC_{50}), or (d) combination of GS-444217 and enalapril (Supplemental Figure 5E). Rats were treated from week 8 to week 12 after Nx. Treatment with GS-444217 alone did not reduce systolic blood pressure, whereas enalapril alone or in combination with GS-444217 led to a reduction of systolic blood pressure between weeks 8 and 12 (Figure 8A). Albuminuria increased from week 8 to week 12 in vehicle-treated 5/6 Nx rats and was lower in 5/6 Nx rats treated with GS-444217 or enalapril alone (Figure 8B). Notably, the combination of GS-444217 and enalapril decreased albuminuria to concentrations below that observed before treatment and more than either agent alone (Figure 8B). Mean sclerosis index scores increased from biopsy at 8 weeks to autopsy at 12 weeks in vehicle-treated 5/6 Nx rats (Figure 8C and Supplemental Figure 17). The mean percentage change in sclerosis index between biopsy and autopsy for each group was 80.6% ± 14% for vehicle, 65% ± 13% for enalapril, 45.6% ± 23% for GS-444217, and 19% ± 13% for the combination of GS-444217 and enalapril (Figure 8, C and D). Further, 4 of 12 rats treated with the combination of GS-444217 and enalapril showed evidence of regression of glomerulosclerosis, i.e., less sclerosis at autopsy than at biopsy, compared with worsened glomerulosclerosis in all vehicle-treated rats (Supplemental Figure 17).

In summary, in a setting of severe hypertension, inhibition of ASK1 with GS-444217 exerts beneficial effects on glomerulosclerosis and albuminuria. GS-444217 increased the efficacy of antihypertensive therapy by significantly reducing or regressing the progression of kidney fibrosis in hypertensive rats.

Discussion

We have discovered and characterized GS-444217, a novel inhibitor of ASK1 with good kinase selectivity and a unique cross-dimer interaction with ASK1. GS-444217 is an ATP-competitive inhibitor of ASK1 with nanomolar potency in biochemical and cellular assays, has a desirable oral PK profile in rats and mice, and dose-dependently inhibits ASK1 signaling in kidney. At the time of this work, a limited number of ASK1 inhibitors had been disclosed (46–48); the 2 examples of compounds with cellular potency showed activity in the 1–10 μM range (49, 50), highlighting the need to identify ASK1 inhibitors with improved potency. More recently, 2 new series of ASK1 inhibitors with good cellular potency have been disclosed (51, 52), and both classes of compounds use an amide carbonyl as the hinge binder. To our knowledge, ours is the first report to detail the discovery, pharmacokinetics, pharmacodynamics, and efficacy of a small-molecule inhibitor of ASK1 to reverse end-organ fibrosis and improve renal function. Using multiple acute and chronic preclinical models of kidney injury, we have demonstrated that pharmacological inhibition of ASK1 with GS-444217 is efficacious in reducing key pathological drivers of kidney injury and DKD.

The optimization of compound 1, our initial high-throughput screening hit, was accomplished by manipulation of physicochemical properties to retain a favorable ADME (adsorption, distribution, metabolism, and excretion) profile and integration of the x-ray crystallographic data to direct efforts toward potency improvement. Metrics to gauge ligand efficiency and lipophilic ligand efficiency (LLE, defined as –log IC_{50} [pIC_{50}] – calculated cLogD [cLogD]) are useful tools to help guide the judicious optimization of drug candidates (53). Compared with compound 1, the molecular weight of GS-444217 increased by only about 50%, while the cLogD increased by less than 1 unit and the potency improved by almost 3 orders of magnitude. As a result, the LLE of GS-444217 was improved by over 2 units compared with that of compound 1 (6.5 vs. 4.4). Although the current results demonstrate that GS-444217 has selectivity for ASK1 against 441 other kinases, it is not possible to completely rule out all potential off-target effects. A limitation to the current studies is that we did not test the compound in $ASK1^{-/-}$ mice, so we cannot formally exclude that all the effects of GS-444217 were mediated by ASK1.

Although OS and ROS production have long been considered drivers of diabetic renal damage, therapeutic strategies to directly reduce ROS or to enhance antioxidant capacity (endogenously or exogenously) have not demonstrated clear clinical benefits (8, 11–13). Therapies targeting key cellular events downstream of OS are of interest to avoid the nonspecificity of targeting ROS, which are highly reactive, transient, and widely distributed among various cellular compartments (12, 13). ASK1 is a redox-sensitive kinase that functions at the apex of a signaling cascade to activate the p38 and JNK arms of the MAPK pathway. $ASK1^{-/-}$ mice are protected from pathological organ remodeling and fibrosis in diverse disease settings and have decreased cell loss by apoptosis, decreased macrophage infiltration into tissues, decreased vascular intimal hyperplasia and ROS production, and improved vascular response to vasodilators (34, 54–57). Importantly, $ASK1^{-/-}$ mice develop normally and have no histological evidence of abnormality, suggesting that therapeutic targeting of ASK1 may be feasible to limit the causes of pathological OS and its effects on organ fibrosis and remodeling (54). p38 activity can be regulated by several pathways besides ASK1, such as UV light, osmotic shock, and numerous inflammatory cytokines and growth factors. Our studies using a selective ASK1 inhibitor and studies by others using $ASK1^{-/-}$ mice demonstrate that ASK1 is an important mediator of p38 activation in the setting of chronic kidney injury and DKD. However, other pathways may also contribute to p38 activation and kidney injury in these models and in human DKD.

Using immunohistochemistry and Western blotting, we and others have demonstrated increased p-p38 and p-JNK levels in the glomerulus and tubulointerstitium of renal biopsies from patients with various fibrotic kidney diseases (28, 29, 58–60). In DKD kidney biopsies, p38 activation was associated with α-SMA–positive myofibroblasts, and the degree of positive staining reflected the severity of tubulointerstitial fibrosis (59). Myofibroblasts colocalize in areas of tubulointerstitial fibrosis and are considered the primary collagen-producing cell type during active fibrogenesis (14). ASK1 activation was detected in DKD biopsies using a newly devel-

oped p-ASK1 antibody (Supplemental Figure 13) and confirmed by quantification of p-p38 immunoreactivity in renal biopsies (61). Prominent p-p38 staining detected in areas of tubulointerstitial fibrosis further implicates the ASK1/p38 axis in the development of myofibroblast accumulation and renal fibrosis. In fact, ASK1 deletion or pharmacological inhibition of p38 or JNK is sufficient to prevent myofibroblast accumulation and collagen deposition in models of kidney fibrosis (23, 62). The evidence of ASK1 pathway activation in biopsies from humans with DKD and CKD, along with data demonstrating that ASK1$^{-/-}$ mice are protected from renal injury and fibrosis, provided the basis for our hypothesis that ASK1 presents a promising pharmacological target in DKD.

We first used an acute pharmacodynamic (PD) model of OS to assess the ability of GS-444217 to block ASK1 activation and signaling in the kidney and to establish dose levels of GS-444217 required to inhibit ASK1 signaling in rodent kidney. Auranofin-induced OS has been shown to cause thioredoxin oxidization and to increase JNK and p38 phosphorylation in various cell types (21, 33). Systemic administration of auranofin to rats caused ASK1, p38, and JNK activation in the renal cortex. ASK1 activation and downstream transcription of multiple inflammatory and fibrotic mediators were inhibited by a single dose of GS-444217. Combining PK and renal PD data, we established a goal of maintaining GS-444217 levels above 1.6 μM to enable sustained inhibition of the ASK1 pathway in rodent kidney for subsequent efficacy studies. Because of the known challenges of detecting p-ASK1 in vivo, we did not directly measure p-ASK1 in all models. Therefore, interpretation of data from the rodent models relies on the PK/PD relationships established in the auranofin PD model and on p-p38 used as a surrogate marker of the ASK1 pathway. Given the complexity of DKD pathophysiology, several models using different pathological stimuli to induce renal injury and fibrosis were selected to establish proof of concept that an ASK1 inhibitor could reduce key hallmarks of DKD pathogenesis and progression, namely, tubulointerstitial fibrosis, glomerulosclerosis, podocyte loss, proteinuria, and GFR decline.

Results from 2 rat models of tubular injury (renal I/R and UUO) demonstrate that ASK1 inhibition with GS-444217 prevented tubular necrosis/apoptosis, decreased tubulointerstitial fibrosis, decreased the transcription of proinflammatory and profibrotic signaling (*Ccl2*, *Cxcl2*, *Il1b*, *Il6*, *Tnfa*, and *Tgfb1* mRNA), and preserved renal function. These data support a critical role for ASK1 in tubular injury and agree with a recent report identifying tubule cells as the primary site of p38 and JNK activation in mice subjected to renal I/R and UUO injury (23). Reductions in tubulointerstitial fibrosis are particularly important for assessing therapeutic potential of ASK1 inhibition, as the degree of tubulointerstitial fibrosis is a strong predictor of CKD progression and GFR decline in humans (5, 35–37). The beneficial effects of GS-444217 in the renal I/R and UUO models are consistent with reports of efficacy in similar models using small-molecule inhibitors of p38 (27, 60, 63, 64). These studies linked inhibition of p-p38 in renal tubular cells with reductions in TGF-β–induced expression of profibrotic and proinflammatory genes (procollagen, *Ctgf*, *Timp1*, *Ccl2*), and with decreases in interstitial myofibroblast accumulation. The reduction in p-p38 and these same signaling pathways following GS-444217 treatment implicates ASK1 as an upstream mediator of tubulointerstitial fibrosis and injury. The efficacy of GS-444217 in these models also demonstrates that selective pharmacological inhibition of ASK1 can reduce renal inflammation, fibrosis, and apoptosis comparably to the protection observed in ASK1$^{-/-}$ mice subjected to similar injury (23, 34).

GS-444217 was evaluated in the db/db eNOS$^{-/-}$ mouse model, which recapitulates several, but not all, features of human DKD, including progressive GFR decline (38, 41). The intensity and distribution of p-p38 IHC in kidneys from db/db eNOS$^{-/-}$ mice were similar to what was observed in p-p38 IHC in kidney biopsies from DKD patients and were completely abolished by GS-444217 treatment. GS-444217, administered for 8 weeks to mice with established renal dysfunction and fibrosis, was efficacious in arresting progressive GFR decline, glomerulosclerosis, and proteinuria. In DKD patients, reductions in glomerular podocyte number predict disease progression and directly contribute to glomerulosclerosis, proteinuria, and loss of renal function (4, 65). GS-444217 treatment halted the ongoing loss of glomerular podocytes in db/db eNOS$^{-/-}$ mice with established disease. A likely mechanism for podocyte protection with GS-444217 is decreased OS-induced apoptosis. This is based on the observation that treatment with GS-444217 reduced apoptosis throughout the kidney in several rodent models of kidney disease, and ROS-induced apoptotic-cell death and activation of p38 are implicated in podocyte loss (66, 67). The improvements in urinary EGF, KIM-1, and TIMP-1 are consistent with improved renal function and reduced renal injury and inflammation and may represent clinically translatable biomarkers that can be modulated by ASK1 inhibition therapy.

To test whether ASK1 inhibition could increase the efficacy of RAS inhibition in established kidney disease, 5/6 Nx rats were treated with GS-444217 alone or in combination with enalapril starting after established glomerulosclerosis was confirmed (8 weeks after Nx). GS-444217 treatment slowed progressive glomerular injury caused by the loss of functional nephrons, which is the final common pathway for CKD regardless of etiology (68, 69). In contrast to the effects of GS-444217, administration of a p38 inhibitor to 5/6 Nx rats has been shown to worsen both glomerulosclerosis and renal function (70). Although the p38 inhibitor used may not be selective or may have off-target effects, these differing results are likely due to the fundamental difference between directly inhibiting p38, which has important roles in normal physiology, and inhibiting a single upstream regulator of p38 that is selectively activated by OS. Indeed, selective ASK1 blockade does not prevent renal p38 activation in response to IL-1β, TNF-α, or LPS administration (23).

GS-444217 treatment slowed the progression of glomerulosclerosis and decreased proteinuria in 5/6 Nx rats without affecting systemic hypertension, a common comorbidity and risk factor for DKD progression. These data are consistent with previous studies in conscious rats and in ASK1$^{-/-}$ mice demonstrating the lack of a role for ASK1 in regulating cardiovascular hemodynamics (71, 72). 5/6 Nx rats treated with the combination of GS-444217 and enalapril demonstrated further decreases in proteinuria and minimal increases in glomerulosclerosis as compared with either agent alone. These results suggest that the ASK1 pathway is orthogonal to the RAS system in the kidney and indicate that ASK1 inhibition may provide additional benefits when administered concomitantly with angiotensin-converting enzyme inhibitors in the setting of reduced nephron function.

In conclusion, GS-444217 is a potent and selective small-molecule inhibitor of ASK1 that is orally available and well tolerated in rodents. Our results from several in vivo models, which collectively represent key hallmarks of acute and chronic kidney diseases, establish ASK1 as a critical mediator of renal fibrosis, apoptosis, and inflammation. Rodents receiving preventive or therapeutic administration of GS-444217 had reduced ASK1 and/or p38 activation in kidney, tubulointerstitial fibrosis and apoptosis, glomerulosclerosis, and proteinuria, and had improved renal function. Taken together, our data support ASK1 as a therapeutic target to reduce kidney injury and fibrosis in renal disease. Selonsertib, a first-in-class ASK1 inhibitor, demonstrated antifibrotic efficacy in a phase II study in patients with nonalcoholic steatohepatitis (NCT02466516; ref. 73) and was also investigated in a phase II study in patients with DKD (NCT02177786, ClinicalTrials.gov; ref. 74). When available, the data from DKD patients will be key to understanding the potential clinical benefits of ASK1 inhibition in patients with CKD.

Methods

Medicinal chemistry

See the Supplemental Methods for additional details on the methods.

Surface plasmon resonance

Binding studies were conducted using the ProteOn XPR36 protein interaction array system (Bio-Rad) in running buffer containing 50 mM HEPES pH 7.5, 150 mM NaCl, 10 mM $MgCl_2$, 0.01% Brij-35, 1 mM TCEP, 5% glycerol, and 1% DMSO at 25°C. Either a general layer high-capacity (GLH) or a general layer medium-capacity (GLM) sensor chip was first preconditioned with injections of 10% DMSO, 0.5% SDS, 50 mM NaOH, and 100 mM HCl in distilled water. The surface was then activated by 20 mM EDAC (1-ethyl-3-[3-dimethylaminopropyl]carbodiimide hydrochloride) and 5 mM sulfo-NHS (*N*-hydroxysulfosuccinimide) from the ProteOn Amine Coupling Kit. Purified dephosphorylated ASK1 was dissolved in 10 mM sodium acetate pH 5.5 at 30 μg/ml and incubated with staurosporine (10 μM) to protect the binding site, and then injected onto the chip surface for immobilization. Unconjugated amine-reactive sulfo-NHS ester was blocked by injection of 1 M of ethanolamine-HCl. Multiple buffer injection cycles were used to allow sufficient time for staurosporine to dissociate from ASK1. A 5-point DMSO concentration series (ranging from 0.8% to 1.2% DMSO) was included to generate a calibration curve and correct for excluded volume effects. GS-444217 (0, 0.125, 0.5, 2, 8, 32 nM) was injected for 240 seconds to monitor the association; compound dissociation was monitored for 1,200 seconds. Data analysis was performed with the ProteOn Manager software (version 3.1.0.6). Sensorgrams were corrected for solvent effects and double-referenced using a channel without protein and the 0 nM compound concentration. Data were fitted using the Langmuir 1:1 model with a term for mass transfer. Values cited for k_{on}, k_{off}, and K_D represent averages and SDs calculated from 4 separate surfaces derived from 2 independent experiments.

KINOME*scan*

The selectivity of GS-444217 was evaluated using KINOME*scan* as previously described (75) and according to the vendor's standard protocol (DiscoverX).

BioMAP Diversity PLUS panel

The activity of GS-444217 was evaluated using the BioMAP Diversity PLUS panel (Supplemental Figure 4A) according to the manufacturer's standard protocol (DiscoverX) as previously described (76, 77). GS-444217 was first tested at 1.111 μM, 3.333 μM, 10 μM, and 370.37 nM and then tested at 10 μM and directly compared with 10 μM BIRB-796, a selective p38 inhibitor (Selleck Chemicals).

ASK1 autophosphorylation and ASK1-mediated signaling in HEK293T cells

Human embryonic kidney cells (HEK293T; ATCC) were infected with full-length human ASK1 adenovirus or with an inactive truncated ASK1 adenovirus (K709R mutant with N-terminally truncated protein) as a negative control using the following conditions: (a) dose response: cells were infected for 24 hours followed by incubation for 2 hours with 0.001, 0.003, 0.01, 0.03, 0.1, 0.3, 1, 3, and 10 μM GS-444217; (b) kinetics: after cells were infected for 24 hours, 1 μM GS-444217 was added to cells for 1, 5, 10, or 30 minutes or 1, 2, or 4 hours; (c) off-rate kinetics: cells were infected for 24 hours followed by incubation with GS-444217 for 30 minutes. After 30 minutes, medium was replaced with serum-free medium without compound and incubated for 0, 10, or 30 minutes or 1, 2, or 4 hours.

Western blot. After each time point, cells from 2 wells were lysed in 1% Triton buffer supplemented with Halt Phosphatase Inhibitor cocktail (Pierce Biotechnology) and cOmplete Mini Protease Inhibitor Cocktail Tablets (Roche Applied Sciences). Protein was quantified using the Bradford method. Twenty micrograms of protein per sample was fractionated on a 4%–12% Bis-Tris gel and transferred to a nitrocellulose membrane using iBlot (Thermo Fisher Scientific). Membranes were blocked in Odyssey blocking buffer (LI-COR Biosciences) and incubated with primary antibodies overnight at 4°C. Membranes were washed in Odyssey blocking buffer and incubated with secondary antibodies for 1 hour, washed, and imaged (Odyssey CLx infrared imaging system, LI-COR Biosciences). Primary antibodies were anti-ASK1 (18-785-210021, GenWay Biotech Inc.), p-ASK1 (3765, Cell Signaling), p-p38 MAPK (9211, Cell Signaling), phospho-MKK3/MKK6 (9231, Cell Signaling), phospho-SEK1/MKK4 (4514, Cell Signaling), P-SAPK/JNK (9251, Cell Signaling), and GAPDH (sc-32233, Santa Cruz Biotechnology). Secondary antibodies were donkey anti–rabbit 800CW (926-32213, LI-COR Biosciences) and goat anti–mouse 680RD (926-68070, LI-COR Biosciences). Antibody dilutions were 1:1,000 except for GAPDH, which was 1:10,000.

Formulation of chow with GS-444217

GS-444217 was homogeneously incorporated into Purina chow 5001 by Research Diets Inc. before being pelleted. A concentration of 0.3% was selected to cover the EC_{50} for inhibiting auranofin-induced ASK1 signaling in the mouse at trough (based on pilot PK experiments, data not shown).

Auranofin in vivo pharmacodynamic model

Administration of auranofin. Male Sprague-Dawley rats (176–200 g, 7–8 weeks old; Charles River Laboratories) received a single oral (p.o.) dose of GS-444217 (10 mg/kg, $n = 14$; 30 mg/kg, $n = 8$–12) or an equal volume of vehicle (p.o., $n = 5$) 30 minutes before administration of auranofin (30 mg/kg, i.p.; Enzo Life Sciences) (experimental outline: Supplemental Figure 5A). Kidney cortex samples were collected 30

minutes later to measure p-ASK1, p-p38, and p-JNK by Western blotting, *Il1b*, *Ccl2*, and *Cxcl2* mRNA expression by reverse transcription PCR, and caspase-3 activity by enzymatic assay. Plasma was collected from individual rats over the course of the dosing interval for PK/PD. p-p38 was measured by ELISA in renal cortex lysates according to the manufacturer's instructions (Exocell Inc.).

Western blot. Kidney cortex was lysed in urea lysis buffer containing Halt Protease Inhibitor cocktail. Lysates were separated by centrifugation, and supernatants were collected in a fresh tube for protein quantitation using the Bradford method. Twenty-five micrograms protein per sample was loaded in wells of 4%–20% Tris-glycine gradient gels for protein separation using mini-gel electrophoresis, and the proteins were transferred from gradient gel onto PVDF membranes by wet method. Membranes were washed, blocked in 5% nonfat dry milk, and probed with 1:1,000 dilution with primary antibodies rocking overnight at 4°C. Membranes were washed and then incubated with secondary antibody at 1:2,000 dilution in 2.5% nonfat dry milk for 1 hour. Membranes were washed, and then Femto chemiluminescence substrate (Thermo Fisher Scientific) was added to the membranes for 5 minutes for detection of HRP-enzyme activity. Images were captured (LAS-3000 imager, FujiFilm Inc.) and quantified (Multi Gauge software, FujiFilm Inc.). Antibodies were rabbit polyclonal phospho–Th838-ASK1 (Gilead Sciences Inc.), p-p38 (9211S, Cell Signaling), p-JNK (9251S, Cell Signaling), IP90 (sc-11397, Santa Cruz Biotechnology), and Femto chemiluminescent substrate (34096, Thermo Fisher Scientific).

Rat renal ischemia/reperfusion injury model

Male Sprague-Dawley rats (176–200 g, 7–8 weeks old; Charles River Laboratories) were randomly assigned to weight-matched treatment groups: (a) sham procedure, $n = 8$; (b) ischemia 30 minutes, $n = 8$; (c) ischemia 30 minutes plus GS-444217 (30 mg/kg, p.o.), $n = 8$. Bilateral renal occlusion was performed on anesthetized rats held at 37°C for 30 minutes. After recovering from anesthesia, rats were placed in metabolic cages for a 24-hour collection of urine. Sham rats underwent midline incision with surgery duration of 30 minutes but were not subjected to occlusion. Necropsy was performed on all rats 24 hours after surgery to collect kidneys and blood (experimental outline: Supplemental Figure 5B). Renal I/R studies were performed at Physiogenix Inc. Serum was analyzed for creatinine and blood urea nitrogen concentrations on a clinical chemistry analyzer. The right kidney was fixed in formalin and stained with H&E to assess tubular necrosis by pathology and with TUNEL to detect apoptotic cells.

Rat unilateral ureteral obstruction model

Male Sprague-Dawley rats (180–205 g; Monash University Animal Research Facility) underwent sham surgery or surgery to permanently obstruct the left ureter as previously described (78). Treatment groups were (a) sham surgery ($n = 4$); (b) UUO surgery, no treatment ($n = 8$); (c) UUO surgery and vehicle (equal volume, p.o., twice daily, $n = 8$); and (d) UUO surgery and GS-444217 (30 mg/kg, p.o., twice daily, $n = 8$). Treatment began 1 hour before UUO and continued for 7 days when all renal tissue was collected (experimental outline: Supplemental Figure 5C). UUO studies were performed at Monash Medical Centre. Methods and reagents were used as previously described (60).

p-p38 immunohistochemistry in human renal biopsies and db/db eNOS$^{-/-}$ mouse kidneys

Formalin-fixed paraffin-embedded renal biopsies from 10 patients with DKD and from 7 donors without kidney disease ("healthy") were obtained from Folio Biosciences. Kidney sections were prepared from db/db eNOS$^{-/-}$ mice that were treated with 0.3% GS-444217 in chow for 8 weeks ($n = 8$–10). Sections were immunostained for p-p38 using a rabbit p-p38 MAPK mAb (9212S, Cell Signaling). Whole-slide images were quantified (Tissue Studio software, Definiens) and expressed as a cellular H-score, which quantifies stain intensity and distribution. In DKD samples, semiquantification of glomerular injury score (0 to 4) was assessed on periodic acid–Schiff–stained sections, and interstitial fibrosis score (0 to 4) was assessed on Masson's trichrome–stained sections, by a board-certified renal pathologist according to established criteria (75).

db/db eNOS$^{-/-}$ mouse model of DKD

Experiments in db/db eNOS$^{-/-}$ mice were performed as described previously (38) at Vanderbilt University Medical Center. Male and female mice were randomly assigned to treatment groups and fed (a) standard chow until 10 weeks of age (baseline cohort, $n = 8$), (b) standard chow from age 10 to 18 weeks ($n = 12$), or (c) chow containing 0.3% GS-444217 from age 10 to 18 weeks ($n = 10$). Mice were placed in metabolic cages at 14 and 18 weeks of age to collect 24-hour urine samples. After the 18-week urine collection, GFR was measured by inulin-FITC method (38), and mice were euthanized for collection of blood and kidney (experimental outline: Supplemental Figure 5D). Renal cortex was immediately flash-frozen in liquid nitrogen and stored at –80°C for later biochemical analysis and for histopathology by immersion and fixation of tissue in a 4% paraformaldehyde/PBS solution. Total urine protein was measured (Bio-Rad Protein Assay Kit, Bio-Rad Laboratories). Creatinine was analyzed in plasma (Olympus AU400 clinical chemistry instrument, Beckman Coulter Inc.) and in urine (enzymatic mouse creatinine assay kit, 80350, Crystal Chem). Albumin concentrations in urine were measured (mouse microalbuminuria ELISA, Exocell Inc.) according to the manufacturer's instructions.

Histopathology assessment of glomerulosclerosis. Fixed kidney was routinely processed, and sections were stained with periodic acid–Schiff. The severity of sclerosis for each glomerulus was graded by a pathologist blinded to the sample groups. A semiquantitative score (sclerosis index) of 0 to 4+ was determined based on the percentage of lesions: 0, no lesion; 1+, <25% of the glomerulus; 2+, 25%–50%; 3+, 50%–75%; and 4+, >75% of the glomerulus. Average sclerosis index score was obtained by averaging of scores of 80–100 glomeruli per mouse.

Immunostaining procedures: Wilms tumor 1 and collagen IV. Kidney was immersion-fixed and routinely processed, and then paraffin-embedded sections were deparaffinized, hydrated, and microwaved (Wilms tumor 1 [WT-1]) or trypsinized (collagen IV) for antigen retrieval. Endogenous peroxidase was quenched with 3% H_2O_2, and slides were exposed to Power Block (BioGenex Laboratories). Primary antibodies were rabbit anti–rat WT-1 (1:800; ab89901, Abcam) and rabbit anti–mouse collagen IV (1:400; Chemicon). DAB was used as a chromogen (Vectastain ABC kit, Vector Laboratories) and hematoxylin as a counterstain. The results were quantitated by point counting on 40 consecutive ×400 magnification fields or 40 glomeruli.

Immunostaining procedures: TUNEL. Sections of paraffin-embedded tissue were dewaxed and hydrated, quenched in 3% H_2O_2, and

then microwaved for antigen retrieval and treated with proteinase K to expose DNA. Slides were incubated in a reaction solution containing TdT terminal transferase Bio-14-dATP (Gibco, Invitrogen) and One-Phor-All buffer (supplied with TdT terminal transferase; Thermo Fisher Scientific). The reaction was terminated, and slides were incubated in HRP-conjugated anti-biotin labeling solution (ABC Elite kit, Vector Laboratories) and stained with DAB. Quantification of apoptotic cells was performed by counting of TUNEL-positive cells in the renal interstitium in at least 6 random high-power fields.

Rat 5/6 nephrectomy model

Male Sprague-Dawley rats (200–250 g, 8–9 weeks old; Charles River Laboratories) underwent uninephrectomy on the right side and ligation of 2 or 3 main branches of the left renal artery by silk ligature to remove approximately five-sixths renal mass (5/6 Nx; Vanderbilt University Medical Center). Eight weeks later, renal shave biopsies were taken under anesthesia by laparotomy to determine the severity of sclerosis by histopathology. Rats were then stratified into treatment groups based on mean values for glomerulosclerosis, systolic blood pressure, and proteinuria and given (a) standard chow (control, $n = 6$), (b) chow containing 0.3% GS-444217 and 30 mg/kg GS-444217 (once per day, p.o., to cover the in vivo EC_{50}, $n = 7$), (c) standard chow and 50 mg/l enalapril (CDS020548, Sigma-Aldrich) in drinking water ($n = 7$), and (d) chow containing 0.3% GS-444217, 30 mg/kg GS-444217 (once per day, p.o., $n = 8$), and 50 mg/l enalapril in drinking water. 5/6 Nx rats were treated for 4 weeks and then euthanized to analyze kidneys for morphological and molecular parameters (experimental outline: Supplemental Figure 5E). The dose and route of delivery for the angiotensin-converting enzyme inhibitor enalapril have been well characterized in this model and are known to reduce glomerular perfusion pressure (79, 80). Glomerulosclerosis and proteinuria were evaluated as described above for db/db $eNOS^{-/-}$ mice. Change in sclerosis from 8-week biopsy to 12-week autopsy was calculated for each rat. Western blots and immunohistochemistry were performed as described above for the db/db $eNOS^{-/-}$ model.

Blood pressure. Systolic blood pressure was measured in conscious rats by tail-cuff impedance plethysmography (BP-2000 Blood Pressure Analysis System, Visitech Systems). Rats were acclimated to the procedure before study data were collected. Mean values were based on the average of 10 stable readings.

Statistics

Data are expressed as the mean ± SEM or SD. The number of replicates for each experiment is stated in Methods and in the figure legends. Statistical differences between 2 groups were evaluated using a 2-tailed *t* test. Multiple-group comparisons were evaluated using 1-way ANOVA followed by Bonferroni's or Newman-Keuls multiple-comparisons tests. Statistical analysis was performed with GraphPad Prism 6 software. A *P* value of less than 0.05 was considered statistically significant.

Study approval

All rodent experiments were performed in accordance with the *Guide for the Care and Use of Laboratory Animals* published by the National Research Council (National Academies Press, 2011). Unless otherwise noted, rats and mice were allowed ad libitum access to food and water, housed under standard conditions, and allowed to acclimate for 7 days before study. Experimental procedures were approved by the IACUC of Gilead Sciences (Palo Alto, California, USA), Physiogenix Inc. (Milwaukee, Wisconsin, USA), or Vanderbilt University Medical Center (Nashville, Tennessee, USA), or approved by the Monash Medical Centre Animal Ethics Committee (Clayton, Australia) and performed in accordance with Australian National Health and Medical Research Council guidelines for animal experimentation.

Author contributions

JTL, BKC, GTN, EBL, GB, SSB, FHK, ML, HY, FYM, TA, SP, SW, MW, GAP, LC, DF, TS, and EH designed and performed experiments, analyzed and interpreted data, and wrote the manuscript. KAK, DJNP, BS, ABF, and DGB designed experiments, analyzed and interpreted data, and wrote the manuscript. MG designed experiments and analyzed and interpreted data. All authors were involved in critically revising the manuscript.

Acknowledgments

We thank Cynthia Willis for editorial assistance and manuscript preparation and David Newstrom and Vivian Barry for technical assistance with immunohistochemistry. All funding was provided by Gilead Sciences.

Address correspondence to: John T. Liles, Department of Biology, Gilead Sciences, 333 Lakeside Drive, Foster City, California 94404, USA. Phone: 650.235.3205; Email: john.liles@gilead.com.

1. Breyer MD, Susztak K. The next generation of therapeutics for chronic kidney disease. *Nat Rev Drug Discov*. 2016;15(8):568–588.
2. Fernandez-Fernandez B, Ortiz A, Gomez-Guerrero C, Egido J. Therapeutic approaches to diabetic nephropathy — beyond the RAS. *Nat Rev Nephrol*. 2014;10(6):325–346.
3. Evans M, Bain SC, Hogan S, Bilous RW, Collaborative Study Group participants. Irbesartan delays progression of nephropathy as measured by estimated glomerular filtration rate: post hoc analysis of the Irbesartan Diabetic Nephropathy Trial. *Nephrol Dial Transplant*. 2012;27(6):2255–2263.
4. Reidy K, Kang HM, Hostetter T, Susztak K. Molecular mechanisms of diabetic kidney disease. *J Clin Invest*. 2014;124(6):2333–2340.
5. Najafian B, Alpers CE, Fogo AB. Pathology of human diabetic nephropathy. *Contrib Nephrol*. 2011;170:36–47.
6. Small DM, Coombes JS, Bennett N, Johnson DW, Gobe GC. Oxidative stress, anti-oxidant therapies and chronic kidney disease. *Nephrology (Carlton)*. 2012;17(4):311–321.
7. Dounousi E, et al. Oxidative stress is progressively enhanced with advancing stages of CKD. *Am J Kidney Dis*. 2006;48(5):752–760.
8. Singh DK, Winocour P, Farrington K. Oxidative stress in early diabetic nephropathy: fueling the fire. *Nat Rev Endocrinol*. 2011;7(3):176–184.
9. Brownlee M. The pathobiology of diabetic complications: a unifying mechanism. *Diabetes*. 2005;54(6):1615–1625.
10. Chao CT, Chiang CK. Uremic toxins, oxidative stress, and renal fibrosis: an interwined complex. *J Ren Nutr*. 2015;25(2):155–159.
11. Jha JC, Banal C, Chow BS, Cooper ME, Jandeleit-Dahm K. Diabetes and kidney disease: role of oxidative stress. *Antioxid Redox Signal*. 2016;25(12):657–684.
12. Schmidt HH, et al. Antioxidants in translational medicine. *Antioxid Redox Signal*. 2015;23(14):1130–1143.
13. Murphy MP. Antioxidants as therapies: can we improve on nature? *Free Radic Biol Med*. 2014;66:20–23.
14. Wang YY, et al. Macrophage-to-myofibroblast transition contributes to interstitial fibrosis in chronic renal allograft injury. *J Am Soc Nephrol*. 2017;28(7):2053–2067.
15. Ichijo H, et al. Induction of apoptosis by ASK1, a mammalian MAPKKK that activates SAPK/

JNK and p38 signaling pathways. *Science*. 1997;275(5296):90–94.
16. Takeda K, Noguchi T, Naguro I, Ichijo H. Apoptosis signal-regulating kinase 1 in stress and immune response. *Annu Rev Pharmacol Toxicol*. 2008;48:199–225.
17. Fujisawa T, Takeda K, Ichijo H. ASK family proteins in stress response and disease. *Mol Biotechnol*. 2007;37(1):13–18.
18. Fujino G, et al. Thioredoxin and TRAF family proteins regulate reactive oxygen species-dependent activation of ASK1 through reciprocal modulation of the N-terminal homophilic interaction of ASK1. *Mol Cell Biol*. 2007;27(23):8152–8163.
19. Zhang R, et al. Thioredoxin-2 inhibits mitochondria-located ASK1-mediated apoptosis in a JNK-independent manner. *Circ Res*. 2004;94(11):1483–1491.
20. Saitoh M, et al. Mammalian thioredoxin is a direct inhibitor of apoptosis signal-regulating kinase (ASK) 1. *EMBO J*. 1998;17(9):2596–2606.
21. Bachnoff N, Trus M, Atlas D. Alleviation of oxidative stress by potent and selective thioredoxin-mimetic peptides. *Free Radic Biol Med*. 2011;50(10):1355–1367.
22. Sturchler E, Feurstein D, McDonald P, Duckett D. Mechanism of oxidative stress-induced ASK1-catalyzed MKK6 phosphorylation. *Biochemistry*. 2010;49(19):4094–4102.
23. Ma FY, Tesch GH, Nikolic-Paterson DJ. ASK1/p38 signaling in renal tubular epithelial cells promotes renal fibrosis in the mouse obstructed kidney. *Am J Physiol Renal Physiol*. 2014;307(11):F1263–F1273.
24. Rui HL, Wang YY, Cheng H, Chen YP. JNK-dependent AP-1 activation is required for aristolochic acid-induced TGF-β1 synthesis in human renal proximal epithelial cells. *Am J Physiol Renal Physiol*. 2012;302(12):F1569–F1575.
25. Lim AK, et al. Role of MKK3-p38 MAPK signalling in the development of type 2 diabetes and renal injury in obese db/db mice. *Diabetologia*. 2009;52(2):347–358.
26. Ma FY, Tesch GH, Flavell RA, Davis RJ, Nikolic-Paterson DJ. MKK3-p38 signaling promotes apoptosis and the early inflammatory response in the obstructed mouse kidney. *Am J Physiol Renal Physiol*. 2007;293(5):F1556–F1563.
27. Prakash J, et al. Intracellular delivery of the p38 mitogen-activated protein kinase inhibitor SB202190 [4-(4-fluorophenyl)-2-(4-hydroxyphenyl)-5-(4-pyridyl)1H-imidazole] in renal tubular cells: a novel strategy to treat renal fibrosis. *J Pharmacol Exp Ther*. 2006;319(1):8–19.
28. Verzola D, et al. Apoptosis in the kidneys of patients with type II diabetic nephropathy. *Kidney Int*. 2007;72(10):1262–1272.
29. Adhikary L, et al. Abnormal p38 mitogen-activated protein kinase signalling in human and experimental diabetic nephropathy. *Diabetologia*. 2004;47(7):1210–1222.
30. Tobiume K, et al. ASK1 is required for sustained activations of JNK/p38 MAP kinases and apoptosis. *EMBO Rep*. 2001;2(3):222–228.
31. Copeland RA. Chapter 8: Reversible inhibitors. In: *Enzymes: A Practical Introduction to Structure, Mechanism, and Data Analysis*. 2nd ed. Hoboken, New Jersey, USA: Wiley; 2000:266–304.
32. Umar S, Hedaya O, Singh AK, Ahmed S. Thymoquinone inhibits TNF-α-induced inflammation and cell adhesion in rheumatoid arthritis synovial fibroblasts by ASK1 regulation. *Toxicol Appl Pharmacol*. 2015;287(3):299–305.
33. Cohen-Kutner M, et al. Thioredoxin-mimetic peptides (TXM) reverse auranofin induced apoptosis and restore insulin secretion in insulinoma cells. *Biochem Pharmacol*. 2013;85(7):977–990.
34. Terada Y, et al. Important role of apoptosis signal-regulating kinase 1 in ischemic acute kidney injury. *Biochem Biophys Res Commun*. 2007;364(4):1043–1049.
35. Zeisberg M, Neilson EG. Mechanisms of tubulointerstitial fibrosis. *J Am Soc Nephrol*. 2010;21(11):1819–1834.
36. Nath KA. Tubulointerstitial changes as a major determinant in the progression of renal damage. *Am J Kidney Dis*. 1992;20(1):1–17.
37. Gilbert RE, Cooper ME. The tubulointerstitium in progressive diabetic kidney disease: more than an aftermath of glomerular injury? *Kidney Int*. 1999;56(5):1627–1637.
38. Zhao HJ, et al. Endothelial nitric oxide synthase deficiency produces accelerated nephropathy in diabetic mice. *J Am Soc Nephrol*. 2006;17(10):2664–2669.
39. Hodgin JB, et al. Identification of cross-species shared transcriptional networks of diabetic nephropathy in human and mouse glomeruli. *Diabetes*. 2013;62(1):299–308.
40. Mohan S, et al. Diabetic eNOS knockout mice develop distinct macro- and microvascular complications. *Lab Invest*. 2008;88(5):515–528.
41. Lim BJ, Yang HC, Fogo AB. Animal models of regression/progression of kidney disease. *Drug Discov Today Dis Models*. 2014;11:45–51.
42. Ju W, et al. Tissue transcriptome-driven identification of epidermal growth factor as a chronic kidney disease biomarker. *Sci Transl Med*. 2015;7(316):316ra193.
43. Musiał K, Zwolińska D. Pleiotropic functions of TIMP-1 in patients with chronic kidney disease. *Cell Mol Life Sci*. 2014;71(8):1547–1548.
44. Coca SG, et al. Plasma biomarkers and kidney function decline in early and established diabetic kidney disease. *J Am Soc Nephrol*. 2017;28(9):2786–2793.
45. Ots M, Mackenzie HS, Troy JL, Rennke HG, Brenner BM. Effects of combination therapy with enalapril and losartan on the rate of progression of renal injury in rats with 5/6 renal mass ablation. *J Am Soc Nephrol*. 1998;9(2):224–230.
46. Okamoto M, et al. Identification of novel ASK1 inhibitors using virtual screening. *Bioorg Med Chem*. 2011;19(1):486–489.
47. Singh O, et al. Crystal structures of ASK1-inhibtor complexes provide a platform for structure-based drug design. *Protein Sci*. 2013;22(8):1071–1077.
48. Volynets GP, et al. Identification of 3H-naphtho [1,2,3-de]quinoline-2,7-diones as inhibitors of apoptosis signal-regulating kinase 1 (ASK1). *J Med Chem*. 2011;54(8):2680–2686.
49. Guo X, et al. Regulation of the severity of neuroinflammation and demyelination by TLR-ASK1-p38 pathway. *EMBO Mol Med*. 2010;2(12):504–515.
50. Terao Y, et al. Design and biological evaluation of imidazo[1,2-a]pyridines as novel and potent ASK1 inhibitors. *Bioorg Med Chem Lett*. 2012;22(24):7326–7329.
51. Gibson TS, et al. Structure-based drug design of novel ASK1 inhibitors using an integrated lead optimization strategy. *Bioorg Med Chem Lett*. 2017;27(8):1709–1713.
52. Lanier M, et al. Structure-based design of ASK1 inhibitors as potential agents for heart failure. *ACS Med Chem Lett*. 2017;8(3):316–320.
53. Hopkins AL, Keserü GM, Leeson PD, Rees DC, Reynolds CH. The role of ligand efficiency metrics in drug discovery. *Nat Rev Drug Discov*. 2014;13(2):105–121.
54. Yamaguchi O, et al. Targeted deletion of apoptosis signal-regulating kinase 1 attenuates left ventricular remodeling. *Proc Natl Acad Sci U S A*. 2003;100(26):15883–15888.
55. Tasaki T, et al. Apoptosis signal-regulating kinase 1 deficiency attenuates vascular injury-induced neointimal hyperplasia by suppressing apoptosis in smooth muscle cells. *Am J Pathol*. 2013;182(2):597–609.
56. Yamashita T, et al. Apoptosis signal-regulating kinase-1 is involved in vascular endothelial and cardiac remodeling caused by nitric oxide deficiency. *Hypertension*. 2007;50(3):519–524.
57. Kataoka K, et al. Apoptosis signal-regulating kinase 1 deficiency eliminates cardiovascular injuries induced by high-salt diet. *J Hypertens*. 2011;29(1):76–84.
58. De Borst MH, et al. Glomerular and tubular induction of the transcription factor c-Jun in human renal disease. *J Pathol*. 2007;213(2):219–228.
59. Sakai N, et al. Involvement of extracellular signal-regulated kinase and p38 in human diabetic nephropathy. *Am J Kidney Dis*. 2005;45(1):54–65.
60. Stambe C, Nikolic-Paterson DJ, Hill PA, Dowling J, Atkins RC. p38 Mitogen-activated protein kinase activation and cell localization in human glomerulonephritis: correlation with renal injury. *J Am Soc Nephrol*. 2004;15(2):326–336.
61. Tesch GH, Ma FY, Nikolic-Paterson DJ. ASK1: a new therapeutic target for kidney disease. *Am J Physiol Renal Physiol*. 2016;311(2):F373–F381.
62. Tesch GH, Ma FY, Han Y, Liles JT, Breckenridge DG, Nikolic-Paterson DJ. ASK1 inhibitor halts progression of diabetic nephropathy in Nos3-deficient mice. *Diabetes*. 2015;64(11):3903–3913.
63. Li R, Ding T, Liu X, Li C. Influence of SB203580 on cell apoptosis and P38MAPK in renal ischemia/reperfusion injury. *J Huazhong Univ Sci Technol Med Sci*. 2006;26(1):50–52.
64. Nishida M, Okumura Y, Sato H, Hamaoka K. Delayed inhibition of p38 mitogen-activated protein kinase ameliorates renal fibrosis in obstructive nephropathy. *Nephrol Dial Transplant*. 2008;23(8):2520–2524.
65. Brosius FC, Coward RJ. Podocytes, signaling pathways, and vascular factors in diabetic kidney disease. *Adv Chronic Kidney Dis*. 2014;21(3):304–310.
66. Susztak K, Raff AC, Schiffer M, Böttinger EP. Glucose-induced reactive oxygen species cause apoptosis of podocytes and podocyte depletion at the onset of diabetic nephropathy. *Diabetes*. 2006;55(1):225–233.
67. Lin JS, Susztak K. Podocytes: the weakest link in diabetic kidney disease? *Curr Diab Rep*. 2016;16(5):45.

68. Wang X, Garrett MR. Nephron number, hypertension, and CKD: physiological and genetic insight from humans and animal models. *Physiol Genomics*. 2017;49(3):180–192.
69. Romagnani P, et al. Chronic kidney disease. *Nat Rev Dis Primers*. 2017;3:17088.
70. Ohashi R, et al. Inhibition of p38 mitogen-activated protein kinase augments progression of remnant kidney model by activating the ERK pathway. *Am J Pathol*. 2004;164(2):477–485.
71. Izumiya Y, et al. Apoptosis signal-regulating kinase 1 plays a pivotal role in angiotensin II-induced cardiac hypertrophy and remodeling. *Circ Res*. 2003;93(9):874–883.
72. Budas GR, et al. ASK1 inhibition halts disease progression in preclinical models of pulmonary arterial hypertension. *Am J Respir Crit Care Med*. 2018;197(3):373–385.
73. Loomba R, et al. The ASK1 inhibitor Selonsertib in patients with nonalcoholic steatohepatitis: a randomized, phase 2 trial. *Hepatology*. 2018;67(2):549–559.
74. Lin JH, Zhang JJ, Lin SL, Chertow GM. Design of a phase 2 clinical trial of an ASK1 inhibitor, GS-4997, in patients with diabetic kidney disease. *Nephron*. 2015;129(1):29–33.
75. Tervaert TW, et al. Pathologic classification of diabetic nephropathy. *J Am Soc Nephrol*. 2010;21(4):556–563.
76. Ikoma M, Kawamura T, Kakinuma Y, Fogo A, Ichikawa I. Cause of variable therapeutic efficiency of angiotensin converting enzyme inhibitor on glomerular lesions. *Kidney Int*. 1991;40(2):195–202.
77. Ma LJ, et al. Regression of glomerulosclerosis with high-dose angiotensin inhibition is linked to decreased plasminogen activator inhibitor-1. *J Am Soc Nephrol*. 2005;16(4):966–976.
78. Ciceri P, et al. Dual kinase-bromodomain inhibitors for rationally designed polypharmacology. *Nat Chem Biol*. 2014;10(4):305–312.
79. Berg EL, et al. Chemical target and pathway toxicity mechanisms defined in primary human cell systems. *J Pharmacol Toxicol Methods*. 2010;61(1):3–15.
80. Karaman MW, et al. A quantitative analysis of kinase inhibitor selectivity. *Nat Biotechnol*. 2008;26(1):127–132.